Role of inheritance during tectonic inversion of a rift system in a thick- to thin-skin transition: Analogue modelling and application to the Pyrenean – Biscay System

Jordi Miró[1], Oriol Ferrer[1], Josep Anton Muñoz[1], Gianreto Manastchal[2]

[1]Institut de Recerca GEOMODELS, Departament de Dinàmica de la Terra i de l'Oceà, Facultat de Ciències de la Terra, Universitat de Barcelona, Barcelona, 08028, Spain
[2]Université de Strasbourg, CNRS, ITES UMR 7063, Strasbourg F-67084, France

Correspondence to: Oriol Ferrer (joferrer@ub.edu)

Abstract. The reactivation of former rift systems and passive margins during tectonic inversion and their incorporation into fold-and-thrust belts results in significant structural differences not only between internal to external domains, but also along-strike. The Basque-Cantabrian and Asturian systems are among the best examples to address the role of along-strike changes in rift inheritance since they show a transition from salt to basement inherited structures divided by a transition zone separating thick- from thin-skin structural domains. While both domains have been widely described in the literature, the transfer system separating the two has been yet little investigated due to the poor seismic imaging and the lack of large-scale outcrops. This contribution aims to address the linkage between basement-controlled (i.e., thick-skinned) and salt decoupled (i.e., thin-skinned) domains and to describe how deformation is accommodated in the transitional zone between these domains. An experimental program based on analogue models has been designed that was inspired by the transition from the thin-skinned Basque – Cantabrian Pyrenees to the east to the thick-skinned Asturian Massif to the west. As observed in nature, experimental results show that oblique structures (at low angle with the shortening direction) form in the transitional domain, and their location depends on the linkage of the active structures occurring in both surrounding thick- and thin-skinned domains at different positions. Nevertheless, their orientation and evolution are controlled by the underlying decoupling horizon (i.e., salt). The deformation in the thick-skinned domain produces significant topography over a narrow deformation area due to the lack of effective decoupling levels. On the contrary, deformation in the thin-skinned domain is more distributed due to decoupling, resulting in a wider deformation area of less topography. As a result, syn-contractional sedimentation is occurring mainly in the foreland basin in front of the thick-skinned domain, whereas it is observed in the foreland but also in piggy-back basins in the thin-skinned domain.

1 Introduction

30 The presence of inherited structures and weak horizons at different structural levels are among the most important factors controlling the structural evolution of fold-and-thrust belts (FTB). In mountain belts, reactivated structures are usually inherited from a preceding rift system or a passive margin. Thus, the inherited extensional structural grain must be taken into account for the understanding of the structural style and evolution of FTBs (Carrera et al., 2006, Tugend et al., 2014; Chenin et al., 2017). As a part of the inheritance, the distribution and continuity of weak horizons, such as salt layers, interbedded in

35 the deformed succession also play a significant role in the along-strike variation of the structural style of FTBs as they act as efficient detachment layers [e.g., Zagros (Molinaro et al., 2005, Sherkati et al., 2006, Mouthereau et al., 2007), Sierra Madre Oriental (Marrett and Aranda-García, 2001), Pyrenees (Carola et al., 2013, Jourdon et al., 2020)]. Such along-strike variations are expressed by differences in the structural style and final topography, changes in the vergence, the development of salients and reentrants, and the presence of oblique and transverse structures connecting different segments of the orogen

40 (Jaumé and Lillie, 1988; Cotton and Koyi, 2000; Bahroudi and Koyi, 2003; Muñoz et al., 2013; Ghani et al., 2018).

Inversion tectonics (i.e., positive inversion sensu Cooper et al., 1989) is widely recognized in thick-skinned structural domains, as the basement is usually involved during the contractional reactivation of inherited extensional faults [e.g., Asturian Massif (Pulgar et al., 1999), Andes (Carrera and Muñoz, 2013; Iaffa et al., 2011a and b)]. However, the presence of a salt horizon in the deformed succession can mask inversion tectonics because the absence of diagnostic structural features.

45 Thus, reactivated subsalt basement-involved faults can be laterally shifted and contractional deformation in the cover succession be restricted to the squeezing of pre-existing salt structures, such as observed in the southern North Sea or in the Mid-Polish Trough (Mazur et al., 2005). The timing of salt deposition related to the main extensional episode (i.e., pre- or syn-rift) as well as its regional distribution within a rifted margin will determine the structural style during the subsequent contractional deformation. For a pre-rift salt, the distribution depends on factors such as the initial salt thickness, the amount

50 and rate of extensional deformation, and the erosion/dissolution in the uplifted footwalls (Rowan, 2014). In the case of syn-rift salt, thickness and facies distribution depend on the geometry of the fault system and the interplay between fault throw, sedimentation rate, and depositional conditions (Rowan, 2014). Contractional deformation of a salt-bearing rift system results into a different style of inversion tectonics, dominated by decoupling and squeezing of salt structures [e.g., Pyrenees (Carola et al., 2015; Muñoz et al., 2018), Alps (Granado et al., 2018; Célini et al., 2020)]. In such circumstances, inversion

55 tectonics can be inferred from differences in the stratigraphic record between adjacent structural units and changes of the regional elevation.

Scaled analogue models have been widely used to deal with multiple structural problems in rift systems such as the structural inheritance in extensional oblique rift systems (e.g. McClay and White, 1995; Amilibia et al., 2005); basement-controlled transfer zones (e.g. Acocella et al., 1999; Wu et al., 2009); the inversion of normal faults with evaporites (e.g. Del Ventisette

60 et al., 2006; Sani et al., 2007; Bonini et al., 2012; Ferrer et al. 2016 and submitted; Roma et al., 2018a and b; Dooley and Hudec, 2020; Wilson et al., submitted) and without evaporites (e.g. McClay, 1989; McClay and Buchanan, 1992; Pinto et al.,

2010; Ferrer et al. 2016; Granado et al., 2017); the distribution and impact of salt in thin-skinned extensional settings (e.g. Vendeville and Jackson, 1992a, b; Jackson et al., 1994), and the role of basement faults beneath decoupling horizons (e.g. Withjack and Callaway, 2000; Dooley et al., 2005, Ferrer et al., 2016 and 2023a; Roma et al., 2018a and b; Wilson et al., submitted). On the other hand, no experiments have been conducted addressing the interplay of pre-rift salt and basement structures during formation and inversion of rift systems in a three-dimensional point of view. For this reason, we present a set of 3-D analogue models to investigate how the structural grain inherited from a rifting episode controls the along-strike variation of thick- to thin-skinned deformation in FTBs. Our experimental set-up has been inspired by the Asturian Massif and the Basque – Cantabrian Pyrenees case study, where a transition from a non-salt (i.e., thick-skinned) to a salt dominated system (i.e., thin-skinned) occurs. The experimental protocol presented in this study allows: (1) to understand the along-strike thick- to thin-skinned transition in collisional orogens, (2) to investigate how deformation links both domains in space and time, and (3) to improve the understanding of the transition between the Asturian Massif and the Basque-Cantabrian Pyrenees.

2 Geological setting

The Biscay-Pyrenean domain is located between the southern North Atlantic and the Alpine Tethys (Angrand and Mouthereau, 2021; Asti et al., 2022). This domain is subdivided into several segments that formed during an incomplete Wilson Cycle (Tavani et al., 2018; Chevrot et al., 2018; Manatschal et al., 2021). The segments show a different rift maturity increasing westward, and a slightly to complete reactivation of the former rifted margin/rift system (Tugend et al., 2014). The basement of the studied area was affected by the Variscan orogeny (Martínez-Catalan et al., 2007; Matte, 1991). Subsequently, a post-Variscan extensional collapse preceded a multistage Mesozoic rifting, responsible for the formation of numerous extensional basins along northern Iberia (Roest and Sirvastava, 1991; Roca et al., 2011; Tugend et al., 2015; Cadenas et al., 2020; Frasca et al., 2021; Asti et al., 2022). The extensional evolution was complex, including three rift events: a first, distributed Triassic rifting that was accompanied by the uneven deposition of salt (Cámara and Flinch, 2017; Cámara, 2020; Gómez et al., 2007; López- Gómez et al., 2019), a Late Jurassic to Barremian transtensional rift event linked to narrow but deep depocenters aligned along the nascent and diffuse European-Iberian plate boundary (e.g., Asturian Basin, Cabuérniga Basin, Basque – Cantabrian Basin, etc.) (Cadenas et al., 2020; Tavani et al., 2018; Frasca et al., 2021; Miró et al., 2021; Asti et al., 2022), and a Late Aptian to Cenomanian hyperextended rift system that represents the main extensional event (Roca et al., 2011; Tugend et al., 2014; Pedreira et al., 2015; Cadenas et al., 2020; Miró et al., 2021; Lescoutre et al., 2021). As a result of the successive extensional phases, seafloor spreading took place in the Bay of Biscay, while mantle exhumation occurred along the Ocean Continent Transitions (OCT) on either side and in the less mature North Iberian Rift System to the east (Tugend et al., 2014; Pedrera et al., 2017; García-Senz et al., 2019; Lescoutre et al., 2021).

The present-day architecture of the entire Pyrenean orogen changes significantly along-strike as revealed by the observed differences in the structural style (Fig. 1). The along-strike changes in the orogenic structure may be one of the reasons of a

confusing terminology of the Pyrenean realm (see Miró et al. (2020) for an overview). In this study we used: a) the Pyrenees *s.s.* for the eastern portion of the orogen where Mesozoic basins are located north and south of the Axial Zone, which is made of Palaeozoic rocks representing the higher topography of the mountain belt; b) the Basque–Cantabrian Pyrenees for the central portion of the orogen characterized by the inversion of the Basque–Cantabrian Basin and surrounding minor basins, where Mesozoic rocks crop out, resulting in smoother topography; and c) the Asturian Massif for the western sector characterized by Palaeozoic rocks with a very reduced Mesozoic succession on top but a significant topography to the south and a slightly reactivated extensional system offshore to the north (Fig. 1).

[Figure 1]

Although the rifted margin configuration is fundamental to understand the reactivation and the subsequent evolution of the entire Pyrenean orogenic system during Late Cretaceous to Cenozoic (Muñoz, 1992; Roca et al., 2011; Tugend et al., 2014; Tavani et al., 2018; Frasca et al., 2021; Angrand and Mouthereau, 2021) it is not yet well understood in detail. Some first studies (Roca et al., 2011; Cadenas et al., 2020; Lescoutre and Manatschal, 2020; Saspiturry et al., 2020; Lescoutre et al., 2021; Miro et al., 2021) addressed the study of the reactivation of the inherited rift structures. Numerical models inspired in the Pyrenees have also addressed the reactivation of inherited rift systems at lithospheric scale and explored the differences on the structural style depending on the involvement of weak salt layers (Beaumont et al., 2000; Jourdon et al., 2020; Wolf et al., 2021). All these numerical models are 2D experiments showing a first-order role of the presence of salt in the structural and topographic evolution of orogenic belts at lithospheric scale. Thus, the presence of salt promotes the forward propagation of deformation, the decoupling of supra-salt sequences and formation of piggy-back basins, and reduces the topography, delaying the stratigraphic record of the orogenic deformation (Jourdon et al., 2020; Wolf et al., 2021). These models also explain the main structural differences between the realms of the Pyrenees involving a thick Triassic salt (such as the Basque-Cantabrian Pyrenees) from other realms, where the salt is thin or absent (Asturian massif and eastern Pyrenees) (Jourdon et al., 2020). However, there are still some unanswered questions: How do the transitional domains connect the different segments of the orogen? How did inherited rift structures control the contractional reactivation of the transitional domains? Here we follow a different approach and methodology to understand the role of the rift inheritance to explain the along-strike structural changes in the Pyrenean orogen by means of an experimental approach based on scaled analogue (sandbox) models. To achieve this objective, and differently to the numerical modelling studies above mentioned, we have developed 3D models. This work first addresses a generic problem, which is the along-strike transition from a salt-dominated segment to a segment controlled by basement structures without salt. Our study is inspired by the observations made along the transition between the Basque-Cantabrian and Asturian segments. We mainly focus on the proximal rift domains, which are the areas that never underwent a crustal thinning to less than 25 km thick (Tugend, et al., 2014, Cadenas

et al., 2018) and their later reactivation during the Alpine Orogeny (Roca et al.,2011; Pedreira et al., 2015; García-Senz et al., 2019; Miró et al., 2021) (Fig. 2).

The Basque – Cantabrian Pyrenees are the result of the inversion of the western North Iberian hyperextended Rift System (Roca et al., 2011; Lescoutre and Manatschal, 2020; Cadenas et al., 2020; Miró et al., 2021). The hyperextension was controlled by a north dipping extensional detachment that was subsequently reactivated during the Pyrenean contractional deformation. However, due to the salt detachment inherited from the Late Triassic rift event (López-Gómez et al., 2019; Lagabrielle et al., 2020), the reactivation of the Basque – Cantabrian Pyrenees occurred with a thin-skinned structural style, starting during the Late Cretaceous up to the Oligocene (Riba and Jurado, 1992; Tavani et al., 2013; Carola et al., 2013 and 2015; Cámara and Flinch, 2017; Cámara, 2020; Muñoz, 2019; Lescoutre and Manatschal, 2020; Miró et al., 2021). Consequently, the Mesozoic sedimentary succession of the southern Basque – Cantabrian Pyrenees has been transported over more than 30 km to the south over the foreland basin (Muñoz, 2019; Miró et al., 2021) (section 2, Fig. 2). As a result, in the thrust front, pre-existing salt structures have been reactivated and squeezed during inversion, whereas the ones located to the north into the thrust wedge (i.e., Alavesa Platform) and developed in more distal domains (northern part of the former rift proximal domain and its transition to the necking domain) are still preserved showing none, or only slightly, contractional reactivation (e.g., Salinas del Rosio and Villasana de Mena salt diapirs) (section 2, Fig. 2). The underlying basement is flat in the Duero and Ebro foreland basins whereas slightly dips northward beneath the frontal thrust (Carola et al., 2015; Muñoz, 2019; Miró et al. 2020 and 2021). Other interpretations have been proposed for the Basque – Cantabrian Pyrenees, arguing for a thick-skinned reactivation with no decoupling along the Triassic salt during the contractional deformation (Quintana et al., 2015; Pedrera et al., 2017 and 2020; García-Senz et al., 2019).

145

[Figure 2]

In the Asturian Massif, on the contrary, a consensus exists on the interpretation of the Pyrenean contractional structures. In this area, they consist of a thick-skinned thrust system controlled by the reactivation of inherited Variscan faults (Alonso et al., 1996; Gallastegui, 2000). Triassic salt was either not deposited or completely eroded (López-Gómez et al., 2019) conditioning the thick-skinned structural style. Thus, the area shows a contrasting structural style compared to the Basque – Cantabrian Pyrenees further to the east. The proposed interpretations of the Asturian Massif (e.g., Alonso et al., 1996, Pulgar et al., 1999) show a major mid-crustal sole thrust dipping to the north and getting flat at about 15 km depth acting as an intra-crustal decoupling level for the structures depicted in the hanging wall (section 1, Fig. 2). The fault propagation fold observed at the thrust front involving the Paleogene-Neogene syn-orogenic sediments located at the northern limit of the Duero Basin represents the field expression of this major sole thrust (Pulgar et al., 1999; Gallastegui, 2000).

Between these two main structural domains, a less investigated domain connects the Asturian domain to the west with the Basque – Cantabrian domain to the east (Fig. 2). The transitional domain is characterized by both E-W (e.g., Cabuérniga

Fault) and NW-SE (e.g., Rumaceo and Golobar Faults) major structures that outcrop to the west but sole out to the east, plunging eastwards. These inherited basement-involved structures (Espina, 1996) have been reactivated during both rifting and Pyrenean orogenic phases. In addition, the Upper Triassic salt has an irregular distribution in this transitional domain, being abundant to the north in the Santander Block, with little or no evidence in the Cabuérniga Basin but outcropping again to the south in the Polientes Basin (López-Gómez et al., 2019). Moreover, salt thickness increases to the east (Camara, 2017). Early Cretaceous extensional faults and related salt structures and Lower Cretaceous mini-basins are observed in this domain (García de Cortázar and Pujalte, 1982; Espina, 1994). However, besides some good outcrops, vegetation, poorly imaged and scarce seismic, and drill hole data, which is very poor or absent in most of the transitional domain, makes precise and further investigation difficult.

3 Analogue modelling

3.1 Experimental methodology

The experimental configuration simulates: 1) the distribution of basement-involved structures, aiming to reproduce the inverted extensional faults at the eastern edge of the Asturian Massif (i.e., Cabuérniga and Golobar-Rumaceo faults, Fig. 2), and 2) an uneven distribution of the Upper Triassic salt (Keuper), aiming to reproduce a thick salt layer in the Basque-Cantabrian Pyrenees pinching out towards the Asturian Massif (Fig. 3).

3.1.1 Model set-up

The 3D experimental program was carried out in a 75 cm-long, 70 cm-wide glass-sided deformation box (Fig. 3a). Two mobile end walls orthogonal to the glass-sided walls made the experiment a closed system. Both glass walls were fixed whereas computer-controlled servomotors moved the two metal ones. Two rigid wooden blocks attached to the mobile end walls were used to simulate the inherited basement structures (Figs. 3a and b). Both blocks have a regional dip of 3° to the E. The northern block had a rectangular plan view shape, whereas the southern one was trapezoidal (Figs. 3a and b). In both cases, a surface dipping 60° towards the inner part of the model simulated the E-W Cabuérniga Fault (northern block) and the NW – SE Golobar and Rumaceo Faults (southern block) (Figs. 3a, b, and e). The space between the two blocks was filled with white silica sand keeping the 3° eastwards regional dip and would represent in nature inherited Permian extensional basins (Espina, 1996). Then, a purple sand layer wedging eastwards as the previous materials overlie both blocks and the white sand.

On the other hand, the two rigid blocks change to two flat wooden plates on the eastern side of the rig (Figs. 3a and b). Here, a 19 mm-thick polymer layer pinching out westwards on top of the basement sand wedge simulates the Upper Triassic salt basin at the Basque-Cantabrian Pyrenees (Figs. 3c and d). It has been estimated that the original thickness of the Upper Triassic evaporites is between 500 and 2000 m throughout the basin (Cámara and Flinch, 2017). Finally, a 10 mm-thick blue

sand layer overlaid the polymer layer pinching out westwards against the basement wedge (Figs. 3c, d, and e). According to the polymer distribution, three structural domains can be defined: a) a western coupled domain (or highly coupled domain) without polymer between the basement rigid blocks and the sand representing the sedimentary cover; b) a central transitional domain, where the polymer overlaps the basement blocks; and c) an eastern decoupled domain, where the thickness of the polymer is constant at the base of the sand pack (Fig. 3d). These structural domains will be hereinafter used to facilitate the explanation of the experimental results.

In the model set-up, the western part of the modelled area corresponds to the eastern termination of the Asturian massif where thrusts climb up section from the Variscan basement to the Triassic evaporites of the Basque-Cantabrian Basin eastwards. It has been interpreted that the basal detachment during the Pyrenean contractional deformation in the Asturian massif is located at about 15km or even shallower (Espina, 1996; Pulgar et al., 1999). This basal detachment deepens and wedges northwards rooting into deeper crustal levels (Gallastegui et al., 2016). So, it is part of a thick-skinned system. However, in the eastern part of the Asturian massif, this sole detachment shallows eastwards as imaged by the available seismic lines (Carola et al., 2015) and is consistent with the thickness and geometry of the wooden blocks of the model set-up. In the modelled area we only deal with the shallower part of this thick-skinned system, and it would be represented by the detachment above the rigid basal plate and underneath the wooden blocks in the western part of the model. Thus, we focus on the easternmost part of this thick-skinned system as our aim is to analyze the transition area to the thin-skinned domain located further east. In the set-up of our models, the rigid basal plate is planar, but in nature it would represent a detachment horizon climbing up section eastwards from the basement (rigid blocks) into the salt layer (silicon), that is, from the eastern edge of a thick-skinned domain to a thin-skinned one

[Figure 3]

3.1.2 Analogue materials and scaling

Well-sorted and rounded dry silica sand was used as analogue for brittle rocks in the upper continental crust (Schellart, 2000). On the other hand, a polydimethylsiloxane (PDMS) silicone polymer simulated the behaviour of viscous salt (Weijermars, 1986; Dell'Ertole and Schellart, 2013). The silica sand (white or coloured) with an average grain size of 199 µm obeys a Mohr-Coulomb criterion of failure (Hubbert, 1951; Mandl et al., 1977). The mechanical properties of the poured sand were determined by Roma et al. (2018a) by means of a shear box test, resulting in 34.6°±2° of internal friction, 1500±50 kg·m^{-3} bulk density, 0.69 of internal friction coefficient, and a low apparent cohesive strength of 55 Pa. The PDMS is a near-Newtonian viscous fluid with a density of 972 kg·m^{-3}, a viscosity of $1.6×10^4$ Pa.s, and a strain range of $1.83×10^{-4}$cm·s^{-1} at 20°C (Dell'Ertole and Schellart, 2013). The mechanical properties of the analogue materials and the scaling factors of the experimental program are summarised in Table 1.

Table 1. Scaling parameters used in the experimental program

Parameter	Experiment	Nature	Model ratio
Length (m)	0.01	1000	10^{-5}
Density sand (kg·m^{-3})	1500	2700	0.55
Gravity acceleration (m·s^{-2})	9.81	9.81	1
Density polymer (kg·m^{-3})	972	2200	0.44
Viscosity polymer (Pa·s)	1.6×10^4	10^{15}-10^{19}	$1.6 \times 10^{11/15}$

Table 1: Scaling parameters used in the experimental program.

3.1.3 Procedure

The experimental program presented in this work includes three different experiments (Table 2). Model-1 corresponds to the baseline model to understand what the structural grain was at the end of the extensional episode. Model-2 and Model-3 followed the same extensional evolution as Model-1, but then they were inverted (Table 2). Syn-inversion sedimentation was considered in Model-3 (Table 2).

Table 2. Experimental program

Experiment	Total extension (mm)	Extension rate (mm/h)	Total shortening (mm)	Shortening rate (mm/h)	Syn-comp. sedimentation	Time (hours)
Model - 1	127	3 (N wall) 2 (S wall)	-	-	-	31
Model - 2	127	3 (N wall) 2 (S wall)	200	6 from N 0 from S	-	64
Model - 3	127	3 (N wall) 2 (S wall)	200	6 from N 0 from S	Yes	68

Table 2: Experimental program presented in this work.

The extensional deformation was achieved by moving the two end walls by a servomotor-driven worm-screw controlled by a computer. To produce more accommodation space to the north, where the main depocenter was in the Basque-Cantabrian Basin, the northern wall pulled at a higher velocity (3mm/h) than the southern one (2mm/h). Interbedded layers of white and red sand were used to simulate syn-extensional sedimentation. To favour the early development of salt structures by sedimentary loading and salt evacuation, the first syn-extensional sand layer was poured after 5 hours of extension. All subsequent syn-extensional sand layers were settled every 3 hours. Before the sedimentation of each syn-extensional layer, the rig was tilted 0.35°northwards to simulate the progressive tilting of an extensional rifted margin reaching a regional dip of 2.8° at the end of the extensional phase. At the end of Model-1, the total extension was 127mm (Table 2), (75mm for the northern end wall and 52mm for the southern one), and the resulting basin was filled by 8 syn-extensional sand layers.

After the extensional episode, Model-2 and Model-3 were covered by a 5mm-thick yellow sand layer simulating a post-extensional unit. Both models were subsequently shortened by pushing the northern end wall at a velocity of 6mm/h during 38 hours reaching 200 mm of total shortening. Syn-inversion sedimentation was only considered for Model-3 (Table 2) by alternating green and white sand layers every 3 hours. In addition, after the deposition of each syn-compressional sand layer, the rig was tilted 0.2° to the north up to additional 2.2° to simulate the orogenic flexure of the Basque – Cantabrian Pyrenees (Fig. 2).

The procedure followed during the experiments allowing the tilting of the basal plate during the deformation combined with the limitation of sandbox analogue models when reproducing distinct basement blocks in the deformed materials introduce a simplification in the experiments that must be considered when interpreted the model results. The basal detachment of the thrust wedge coincides with the rigid basal plate of the rig and would represent in nature a detachment horizon climbing up section from the basement westwards into the weak horizon eastwards at the bottom of the cover succession. So, in nature this detachment should show a staircase geometry from the thick-skinned domain where the basement is involved (rigid blocks in the experiments) to the eastern thin-skinned domain where structures decoupled from the basement along the weak salt layer. In the transition from the Asturian massif to the Basque-Cantabrian Basin we may consider that this detachment dips initially westward and gradually climbs up section eastward and thus would not be merely dipping northwards as we have reproduced during the experiments. Adding an additional tilting component would be not possible because the silicon layer would flow in a non-desirable way. In any case, such tilting would not have introduced significant changes in our model results as we focus on the structures that form in the transition between domains as different structures link during the structural evolution.

4 Experimental results

This chapter describes the experimental results of the three models pointing out the kinematics of each deformation phase. Model-1 focuses on the extensional evolution and allows to understand the role of stratigraphic and structural inheritance during the rift phase (Table 2). Model-2 and Model-3 underwent an extensional evolution similar to Model-1 but were subsequently shortened to study how inherited extensional structures were inverted (Table 2). In addition, Model-3 also explores the role of syn-contractional sedimentation during inversion (Table 2). The description of each model has been addressed according to the deformation style of the coupled, transitional, and decoupled structural domains previously introduced (Figs. 3c and d).

4.1 Model-1

Model-1 corresponds to the baseline experiment performed to understand the main extensional elements. During early extension, the experiment shows a strong control of the rigid wooden blocks in the coupled domain, where an E-W trending

graben develops over the edge of the northern block, and a NW–SE trending graben over the southern one (Fig. 4a). In contrast, no structures formed in the decoupled and transitional domains. As extension increases, the northern E-W graben of the coupled domain widened, controlled by a major normal fault rooted at the edge of the rigid block to the north, and a set

275 of two antithetic faults developed to the south (Fig. 4b). Similarly, the southern graben also widened but only a single antithetic fault developed due to the lower extension rate (Fig. 4b). After 25 mm of extension, a wide salt inflation occurred in the central area of the decoupled domain separating two E-W trending grabens at the northern part of the basin and two at the southern one of (Fig. 4b). Triggered by thin-skinned extension, such grabens developed at the top of reactive salt walls. These salt walls evolved to active diapirs with increasing extension (Vendeville and Jackson, 1992a). In the transitional

280 domain, however, four minor grabens relay the two major thick-skinned structures of the coupled domain and the thin-skinned structures of the decoupled domain (Fig. 4b).

[Figure 4]

285 Further extension widens the two grabens of the thick-skinned domain by generating new antithetic normal faults (Figs. 4c and 5a). Progressive northwards tilting of the model during the extensional episode triggered gravitational gliding in the thin-skinned and transitional domains, where the bounding grabens evolve to asymmetric half-grabens controlled by downdip faults (Figs. 5b and 5c). The active salt walls of the decoupled domain evolved to passive diapirs producing small overhangs (Vendeville and Jackson, 1992a; Jackson et al., 1994; Rowan and Giles, 2020) (Figs. 4c and 5c). The wide salt-cored

290 anticline developed at the central position of the decoupled domain is progressively inflated as offlap terminations of the syn-kinematic sand layers indicate (Figs. 4c and 5c). In the meantime, in the transitional domain, the grabens related to the northern structure of the coupled domain were buried and extensional deformation was accommodated in a footwall breached relay ramp linking the northern passive salt wall of the decoupled domain (Fig. 4c). Similarly, a footwall breached relay ramp linked the southern graben of the coupled domain with the southern passive salt wall of the decoupled domain

295 (Fig. 4c).

[Figure 5]

From 70 to 115 cm of extension, the two grabens of the coupled domain widened, and new antithetic faults developed (Figs.

300 4d and 5a). In the decoupled domain, polymer extrusion at the northern passive salt wall ended after 80 mm of extension, when the source layer depleted and primary welds developed. From this point, the northern salt wall became progressively buried by syn-kinematic sedimentation (Figs. 4d and 5c). Further extension widened the diapir producing the roof collapse and the development of a graben (diapir fall sense Vendeville and Jackson, 1992b) (Figs. 4d and 5c). In contrast, the flaring upwards geometry of the southern passive salt wall indicates that extrusion took place until the end of the extension when

305 primary welds developed (Fig. 5c). In the meantime, a graben developed in the crest of the salt-inflated anticline between the two salt walls (Fig. 4d) that will be pierced by polymer developing a new passive salt wall at the last stages of extension (Fig. 5c). Part of the extensional deformation also shifted to the southern polymer pinch out, where a regional dipping extensional fault developed (Fig. 5c). During this episode of deformation, the E-W grabens of the transitional domain became inactive and buried (compare their position in Figs. 5c and 5d). Two new oblique (NW–SE), transtensional grabens

310 developed linking the major grabens of the coupled domain with the new central graben of the salt-inflated anticline and the regional dipping fault developed at the southern polymer pinch out of the decoupled domain (Fig. 4d). Coeval to the formation of the southern transtensional oblique graben, there was a switch in the depocenters location (flip-flop salt tectonics sensu Quirk and Pilcher, 2012). Growth strata clearly indicate that the older depocenter is controlled by the growth of the counter-regional fault. Once the hanging wall of this fault touched down forming a weld, there was a switch of the

315 deformation to the new major regional dipping fault at the southern oblique graben. This change is recorded by a polarity change of growth strata related to both faults, and by the development of an intermediate unconformity (Fig. 5b).

4.2 Model-2

Model-2 followed the same extensional evolution as Model-1, but it was subsequently inverted without syn-contractional

320 sedimentation (Table 1). To avoid repetitions, this section will focus on the description of the results related to the contractional evolution of this model only.

At the end of the extensional episode, the entire model was covered by a 5 mm-thick post-extensional yellow sand layer burying the extensional structures and diapirs. During the onset of shortening, deformation concentrated at the closest structures to the moving wall in the coupled domain. The northern graben in the coupled domain was folded and uplifted by

325 the inversion of the northern master extensional fault and the formation of a foreland-directed thrust nucleated at the base of the rigid block (Figs. 6a and 7). Inversion of the northern graben and its master fault continued into the transitional domain. Moreover, the minor E-W graben and related reactive diapir at the southern edge was also reactivated (compare Figs. 4c, 5a and 6a). In the decoupled domain, shortening progressed further south rejuvenating both the northern and southern salt walls by squeezing, folding and uplifting their roofs (Fig. 6a). Salt pierced the roof at the eastern sector of the northern salt wall

330 and extruded forming a salt sheet (Fig. 6a). During early inversion, the location of the thrust front is constrained by the pre-existing extensional faults and salt structures. It has a W-E trend in the coupled domain and slightly shifts southwards in the decoupled domain. At the transitional domain, both thrust fronts overlap in a soft linkage relaying thick- and thin-skinned domains respectively (Fig. 6a). Part of the contractional deformation propagated to the southern salt wall in the decoupled domain as seen by the salt inflation. Deformation decreases laterally along the intermediate domain, being null in the

335 equivalent coupled domain (Fig. 6a).

[Figure 6]

In further stages of shortening, the height of the northern inverted graben at the coupled domain increases by the emplacement of south-verging thrusts in a piggy-back sequence, but also by the footwall shortcut that develops at the northern edge of the graben (Figs. 6b and 7a). In the decoupled domain, the buried northern salt wall narrows, increasing roof uplift and folding (Fig. 7c). At the eastern termination, the extruding polymer forms a salt sheet that flows down the limbs of the resulting anticline (Fig. 6b). Contractional deformation reaches the southern pinch-out of the salt basin, where an E-W trending foreland-verging thrust developed. The extrusion in the southern salt wall notably increased resulting in a large piggy-back salt sheet confined by the different contractional structures (Fig. 6b). The salt-cored anticline located between the two salt walls is progressively amplified with increasing shortening. The structural complexity of the transitional domain increases as deformation evolved. The northern E-W trending thrust front became rectilinear, linking the foreland-verging thrust of the coupled domain with the foreland-directed thrust nucleated at the top of the buried northern salt wall (Fig. 6b). Further south, the structural style of the transitional domain is strongly controlled by salt thickness. The E-W trend of the decoupled domain structures progressively curves into a NW-SE trend (Fig. 6b). A tear fault developed at the western edge of the salt basin linking the deformation front of the decoupled and coupled domains and segmenting the thrust sheets (Fig. 6b. Southwards of this structure, the E-W trending thrust at the pinch out of the salt basin progressively curves to reach a NW-SE trend in the transitional domain (Fig. 6b).

Increasing shortening forced the rise of a prominent topography in most structures. The southern salt wall of the decoupled domain becomes progressively squeezed developing a secondary weld around 80 mm shortening (Figs. 6c and 7c). After welding, contractional deformation switch from the southern thrust front to the salt-cored anticline northwards of the southern salt wall. This structure is progressively amplified first by buckling and then by the development of a thrust in its southern limb and a back thrust in the northern one (Figs. 6c and 7c). In addition, the southern limb of the anticline experienced a progressive limb rotation, most probably due by a higher friction on the primary weld underneath the secondary one (Figs. 6c and 7c). After 138 mm of shortening the oblique southern graben at the coupled domain is inverted. This is coeval with a continuous slight clockwise vertical axis rotation of the structures at the transitional domain and an increase of the thrust curvature (compare Figs. 6b and 6c). New tear faults trending parallel to the shortening direction develop close to the polymer pinch out at the transitional domain.

From this point until the end of the experiment, shortening amplifies previous structures. In the coupled domain, the orogenic wedge favours the propagation of contractional deformation towards the foreland with the initial inversion of the southern oblique graben, which is subsequently cut out of sequence by the floor thrust of the northern foreland-directed thrust system (Figs. 6d and 7a). In the decoupled domain, shortening amplified the salt-cored anticline developing a crestal collapse graben (Figs. 6d and 7a). During the last stages of deformation, the frontal thrust is reactivated (Fig. 6d). In the transitional domain, contractional deformation is mainly accommodated by the thrust that nucleates at the apex of the reactive diapir inherited from the previous extensional episode (Fig. 4b). This structure links the salt-cored anticline of the decoupled domain with the frontal thrust of the coupled domain (Fig. 6d). At the northwards sector of the transitional

domain, there is also a significant uplift of the graben because of the pre-salt impinging into the overburden (coupled deformation). Part of the deformation is absorbed by the reactivation of the inherited primary weld as a thrust weld.

375

4.3 Model-3

The kinematic evolution of Model-3 during the extensional episode was similar to Model-1 and Model-2, but in this case, sedimentation was added during the inversion episode (Table 1). In order to avoid repetitions, this section will address the

380 most remarkable differences caused by syn-inversion sedimentation.

Despite syn-kinematic sedimentation, the contractional evolution of the three structural domains during early shortening is like in Model-2 (compare Figs. 6a and 8a). The most outstanding differences occur after 70 mm shortening, when syn-contractional sedimentation inhibits the propagation of deformation at the southern salt pinch out as it occurs in Model-2. In this case, shortening is accommodated by the salt-cored anticline northwards of the southern salt wall (Fig. 8b), which for a

385 similar shortening rate reaches a higher topographic relief (Figs. 6b and 8b). The buttressing produced by secondary welding together with the syn-kinematic sedimentation triggered a back thrust, resulting into a more asymmetric anticline than in Model-2 (Figs. 7c and 9c). A new diapir pierces the roof of the northern salt wall that progressively thins by crestal extension as fold growths. The structure of the transitional domain is also slightly different from that of Model-2. The main structure resulted from the westward propagation of the central salt-cored anticline instead of the reactivation of the oblique

390 grabens. The thrust related to this anticline linked with the frontal thrust of the coupled domain along a N-S trending tear fault. (Fig. 8b). In the coupled domain, the oblique southern graben and its propagation towards the transitional domain were rapidly buried by syn-contractional sedimentation without any apparent inversion (Fig. 9b).

395

During the subsequent stages of compression, the major structures of the model are barely amplified. A crestal collapse graben developed in the salt-cored anticline of the decoupled domain (Figs. 8c and 8d). The thrusts emplaced in a piggy-back sequence between 138 and 200 cm of shortening at the coupled domain overthrust the southern graben inhibiting their inversion. New diapirs pierced the crest of the central anticline thinned by a crestal collapse graben at the decoupled domain.

400 Likewise, the volume of polymer at the salt sheets at the end of the experiment is less than in Model-2. The final section of the decoupled domain (Fig. 9c) shows that the northern salt wall is practically welded at the end of the experiment. This fact triggered a greater upwards polymer flow raising and folding the roof, where an incipient crestal collapse graben developed (Fig. 9c).

 [Figure 9]

5 Discussion

5.1 Thick- to thin-skinned transition of the extensional system

Controlled by the experimental setup that includes a western domain with two basal rigid blocks and a décollement layer in
410 the eastern domain, the final structural style shows significant differences along-strike. The coupled domain is characterized
by an extensional fault system nucleated at the rigid block edges simulating E-W and NE-SW-trending major basement-
involved faults bounding a wider graben. Such structural configuration would reproduce a thick-skinned deformation style
with the absence of decoupling between the basement and the cover in the footwall of the main faults. On the contrary, the
decoupled domain, constrained by a salt-equivalent layer underneath the brittle succession, shows a thin-skinned
415 deformation, characterized by E-W-trending structures either during the extensional and subsequent inversion episodes. In
addition, our models are new in the sense that they show the linkage between the structures of the coupled and the decoupled
domains along a transitional domain with a progressive thinning of the salt horizon, and how the inherited extensional
structural grain controls the location of the contractional structures.

During the early extension, the structures developed in the transitional domain are nucleated at the intersection between the
420 edges of the rigid blocks and the polymer pinch out (Fig. 4b). However, their orientation follows the structural trend of the
decoupled domain. This result confirms that even a thin weak horizon may promote decoupling from the inherited basement
features, regardless they may control the location of the supra-salt structures. The location of the structures in the transitional
domain results from the linkage of the structures in the adjacent domains (Fig. 4c). Structures in the coupled domain are
imposed by the basement-involved faults, as reproduced by the fixed wooden blocks. However, the location of the structures
425 in the decoupled domain depends on the ratio overburden/salt thicknesses, the position of the salt pinch-out, and the syn-
tectonic sedimentation. As a result, structures in the decoupled domain extend further and the absence of collinearity with the
structures in the coupled domain results into the development of stepped relay ramps in the transitional domain connecting
parallelly-oriented grabens of the other domains (Figs. 4b and 4c).

Primary welding by salt evacuation in the decoupled domain has a critical impact on the location of new structures as
430 extension increased. Consequently, it affects the trend of the younger extensional faults in the transitional domain. Their
orientation depends on the linkage between the active structures of the decoupled and coupled domains (Fig. 4d). Welding of
the basins adjacent to the salt wall in the decoupled domain promoted the migration of the deformation toward the pinch out
of the salt layer as well as the collapse of the central salt pillow and related salt wall (Fig. 4d). These newly formed
extensional faults, which are in a different position than the former ones, tend to link with the reactivated basement-involved
435 fault at the coupled domain, which remains in a fixed position. As a result, new extensional faults with an oblique trend form

in the transitional domain. Such oblique grabens could be misinterpreted as a subsalt N-S trending strike-slip fault with a dextral displacement.

5.2 Thick- to thin-skinned transition during inversion

440 Two distinct inversion tectonic styles developed in the coupled and decoupled domains as controlled by the reactivation of basement-involved faults and the reactivation of extensional and salt structures respectively. The coupled domain is characterized by a thrust system nucleated in the major extensional faults and a high structural relief given the absence of a weak horizon at the bottom of the thrust wedge. The thin-skinned structural style in the decoupled domain is mainly controlled by the thickness and distribution of salt as well as the location of the salt structures and the extensional faults that

445 triggered them. Synchronous thrusting into the thrust wedge occurred in both domains, although in the decoupled domain the thrust sequence was also controlled by the primary welding of the salt layer as well as by the secondary welding once salt structures were squeezed.

During the contractional deformation, the transitional domain is again the area where oblique and transverse structures develop. However, unlike what occurs in the extensional event, a hard linkage zone developed during the inversion since the

450 early stages of deformation, characterized by N-S trending faults connecting the frontal structures of the coupled and decoupled domains (Figs. 6, 8, and 10).

The inherited salt structures of the decoupled domain are the first to experience contractional deformation during the early stages of inversion synchronously with the inversion of the northern graben of the coupled domain. Buried diapirs are contractionally rejuvenated, squeezed and their overburden folded and uplifted as the inversion of the northern graben of the

455 coupled domain continued (Figs. 6 and 8). In the transitional domain, the first structures to develop are the ones related with the reactivation of the relay grabens and related diapirs, synchronously with the reactivation of the master fault of the northern graben. Immediately afterwards, active structures in the decoupled and coupled domains link, forming N-S trending structures in the transitional domain. This transverse linkage connects active structures and shows different extent and evolution depending on their location, which in their turn is controlled by the inherited extensional and related salt structures

460 and the syn-tectonic sedimentation. Thus, in the model with syn-orogenic sedimentation, the N-S trending element is shorter, as the syn-tectonic sedimentation inhibits the forward propagation of the deformation (compare Figs. 6 and 8). In model-2, the transverse structures consist of two opposed verging thrust salients dissected by a N-S fault, whereas in model-3, a more continuous trending structure developed (compare Figs. 6b and c with Figs. 8b and c). Moreover, in model-2, where deformation progressed forwards both in the decoupled domain (reactivation of the salt pinch out at the thrust front) and in

465 the coupled domain (inversion of the oblique southern graben), the newly formed structures linked also into the transverse N-S system (Fig. 6). Such evolution results into a significant along strike change of this system. Thus, in model-3, the transverse structural element consists of a pop-up bounded by high-angle thrusts in the northern part, whereas further south it corresponds of a shallow dipping thrust with a hanging wall ramp moderately dipping to the west. Such variation occurs in a

very short distance along a continuous structure at surface that could be interpreted as a strike-slip fault (Fig. 10). Thus, a section through the northern part of the N-S structural element could be interpreted as a flower structure (Figs. 10f and 12d and f), whereas the southern edge of the structure corresponds to a lateral ramp of a south-directed thrust linked to the central structure of the decoupled domain (Figs. 10g and 12c and e).

[Figure 10]

Structures with an initially opposed vergence can link, resulting into a single structure with an along-strike change of vergence. An example is the central salt-cored anticline of the decoupled domain that linked with the inverted southern relay graben and related reactive diapir of the transitional domain in both models 2 and 3 (Figs. 6, 8 and 11). The back thrust at the northern limb of the central salt-cored anticline evolves to a pop-up at the boundary between the decoupled and transitional domains and to a forward verging structure into the transitional domain (Fig. 11).

The impact of the syn-contractional sedimentation on the structural evolution of the transitional domain is also notable. Whereas in the model-2 structures striking NW-SE are developed during the early stages of contraction being later crosscut by N-S strike-slip faults (Fig. 6), in model-3 the active structures in both surrounding domains are in a different position resulting in a simpler evolution as explained above governed by N-S orientations.

Thus, the combination of: (1) the location of the inherited salt structures, developed during the extensional episode, and (2) the syn-inversion sedimentation, controlling the location of the active structures in the decoupled domain, determined the orientation and location of the structures at the transitional domain.

[Figure 11]

5.3 Comparison to the Asturian Massif and Basque – Cantabrian Pyrenees

A first order correlation between the models presented in this work and the Asturian and Basque – Cantabrian domains is the regional east plunging structural trend observed in both cases. The Asturian Massif presents higher topography and a narrower deformation zone as it occurs in the western part of the model. Following the Coulomb-wedge theory, the higher basal friction due to the lack of an efficient decoupling level, allows to support more relief. Basal detachment during the Pyrenean contractional deformation in the southern and eastern parts of the Asturian massif is located at upper crustal levels, shallower than 15km, and reactivate former Variscan structures (Espina, 1996; Pulgar et al., 1999; Gallastegui et al., 2016). This basal detachment deepens and wedges northwards rooting into deeper crustal levels. So, it is part of a thick-skinned system. In the modelled area, we only deal with the shallower part of this thick-skinned system, and it would be represented by the detachment above the rigid basal plate and underneath the wooden blocks in the western part of the model. On the contrary, the Basque – Cantabrian Pyrenees present a lower topography and a wider area of deformation as observed in the

eastern part of the model. This is due to the presence of an efficient decoupling horizon (i.e., salt) at the base of the sedimentary succession as demonstrated by many modelling studies since decades ago (Liui Huiqui et al., 1992; Costa and Vendeville, 2002; Bahroudi and Koyi, 2003; Hardy et al., 2009; Wolf et al., 2021, among many others). Therefore, even if the similarity of the model with the observations cannot be used as a proof to support the interpretation proposed here, it shows that the existence of a salt/decoupling horizon may be a prerequisite to obtain the final structures and architecture observed in the transitional area between both domains. This experimental program, as such, is in line with the interpretation of the Basque – Cantabrian Pyrenees as a thin-skinned system in its frontal part, contrary to other models fully controlled by thick-skinned structures (Quintana et al., 2015; Pedrera et al. 2017, 2020; García-Senz et al., 2019), and agrees with recent numerical models (Jourdon et al., 2020).

The transitional domain between the thick-skinned Asturian Massif and the thin-skinned Basque – Cantabrian Pyrenees is characterized by the presence of numerous oblique and transversal structures, as revealed in our models. The main structures in the transitional domain trend mostly N-S to NW-SE and are not consistent with a transpressive inversion model with a NW-SE shortening direction (Tavani et al., 2013). Even more, as shown by the models with the presence of a salt boundary, such structural trends do not require a reactivation of a regional basement transfer feature. In detail, the structures observed in the transitional domain between the Asturian Massif and Basque – Cantabrian Pyrenees are more complicated than the ones reproduced in our models, mainly resulting from the intricate geometry of the Triassic and Late Jurassic-Early Cretaceous rift systems that developed in the area and controlled the distribution of the Triassic salt (López-Gómez et al., 2019, Miró et al., 2021). However, some striking similarities are observed. The Pas thrust system, oriented NW-SE to N-S, connects the western edge of the salt inflated area located north of the Plataforma Burgalesa with the inverted Cabuérniga extensional fault system, where the basement is involved. The hanging wall of the Pas thrust shows a pop-up structure as also revealed by our models (Figs. 9b and 10f). It involves the basement of the transitional domain that has been thrust on top of the coupled domain as partially shown in our models (Fig. 9b). In the section of Fig. 10f the Pas thrust would correspond with the western thrust of the pop-up at the boundary between the transitional and coupled domains. Regardless that in this section it is not the main thrust, it may change along-strike bringing the subsalt succession on top of the salt layer as observed in other sections (Fig. 9b). Along-strike changes of vergence in the transitional and decoupled domains is another feature reproduced in the models and observed also in the field (Figs. 9, 11 and 12). Other oblique features are observed further south in the transitional domain between the Asturian Massif and the Basque-Cantabrian Pyrenees (Fig. 2). They also connect the former salt walls or salt inflated areas located along the southern edge of the Plataforma Burgalesa and the present thrust front with the inverted basement-involved faults of the Asturian massif.

[Figure 12]

A second aspect related to the previous one is the distribution of syn-contractional sedimentation. Whereas in the Asturian Massif (i.e. coupled domain) the syn-contractional sedimentation occurred exclusively in the foreland Duero Basin due to the

orogenic wedge development to the north (Figs. 11c and d) (Pulgar et al., 1999; Alonso, 2007), in the Basque – Cantabrian Pyrenees (i.e. decoupled domain) the distribution of deformation favoured a more distributed topography and therefore a more distributed syn-contractional deformation both in the foreland basin but also in the piggyback basins between the main salt structures (Muñoz, 2019; Jourdon et al., 2020; Miró et al. 2021) (Fig. 11e and f). In between, minor basins with triangular shapes partially controlled by thick-skinned and thin-skinned structures are located (e.g., Cabuérniga and Polientes basins).

6 Conclusions

Using an analogue modelling experimental approach, the aim of this study is to investigate the distribution and evolution of deformation in a thick- to thin-skinned along-strike transition inherited from a rift system during subsequent inversion. The experimental setup has been inspired by observations made in the transition from the autochthonous Asturian Massif to the allochthonous Basque-Cantabrian Pyrenees.

The experimental program presented here demonstrates that the trend and kinematics of oblique structures developed in the transition between domains with and without salt depend on the evolution of active structures in the surrounding thick- and thin-skinned domains. But more importantly, the fact that even a thin low frictional horizon (i.e., the lateral salt pinch–out) may significantly control the structural trend in such positions. The structures in the transitional domain formed by the progressive soft- to hard-linkage of the ones developed in the adjacent domains, which resulted into apparent along-strike changes of geometry and vergence.

Therefore, the experimental results point out the importance of the inheritance: either structural by considering the distribution and orientation of pre-existing basement-involved faults, but also compositional related to the presence and distribution of effective decollement levels. Both aspects have a strong impact on the subsequent contractional evolution of the transitional domain, and the misinterpretation of one of them can introduce significant uncertainties unrevealing the pre-salt geometry.

Finally, the experiments confirm the thick-skinned style controlling the reactivation of the Asturian Massif by creating a narrow thrust wedge with high topography and syn-contractional sediments deposited in the foreland. On the other hand, the models show a wider deformed area to the east with salt structures but with less topographic relief due to the effectiveness of the salt decoupling. This sector is characterized by a more distributed syn-contractional sedimentation both in the foreland and in the deformed domain, similar to what is observed in the Basque – Cantabrian Pyrenees case study.

Acknowledgments

We acknowledge the support of the research project Structure and Deformation of Salt-bearing Rifted Margins (SABREM), PID2020-117598GB-I00, funded by MCIN/ AEI /10.13039/501100011033 and the OROGEN research project. The

GEOMODELS Research Institute and the Grup de Geodinàmica i Anàlisi de Conques (2021SGR76) are also acknowledged for their financial support. The experimental program presented in this work was carried out at the Geomodels Analogue Modelling Laboratory, a Scientific Infrastructure co-funded by the European Regional Development Fund of the Ministerio de Ciencia e Innovación of the Spanish Government (UNBA08-4E-006). We also thank P. Granado, O. Gratacós, M.
570 Snidero, M. Roma, O. Pla, and F. Escosa for logistical support in the modelling laboratory.

References

Acocella, V., Salvini, F., Funiciello, R., and Faccenna, C.: The role of transfer structures on volcanic activity at Campi Flegrei (Southern Italy), J. Volcanol. Geoth. Res., 91(2-4), 123-139, https://doi.org/10.1016/S3077-0273(99)0032-3, 1999.

575 Alonso, J., Pulgar, J., García-Ramos, J., and Barba, P.: Tertiary basins and Alpine tectonics in the Cantabrian Mountains (NW Spain), in: Tertiary Basins of Spain: The Stratigraphic Record of Crustal Kinematics, edited by: Friend, P.F., Dabrio, C.J., Cambrigde University Press, Cambridge, UK, 214-227, https://doi.org/10.1017/CBO9780511524851, 1996.

Alonso, J., Pulgar, J., and Pedreira, D.: El relieve de la Cordillera Cantábrica. Revista de la Asociación Española para la Enseñanza de las Ciencias de la Tierra, 15(2), 151-163, 2007.

580 Amilibia, A., McClay, K.R., Sàbat, F., Muñoz, J.A., and Roca, E.: Analogue modelling of inverted oblique rift systems. Geol. Acta, 3(3), 251-271, https://doi.org/10.1344/105.000001395, 2005.

Angrand, P. and Mouthereau, F.: Evolution of the Alpine orogenic belts in the Western Mediterranean region as resolved by the kinematics of the Europe-Africa diffuse plate boundary, Bsgf - Earth Sci Bulletin, 192, 42, https://doi.org/10.1051/bsgf/2021031, 2021.

585 Asti, R., Saspiturry, N., and Angrand, P.: The Mesozoic Iberia-Eurasia diffuse plate boundary: A wide domain of distributed transtensional deformation progressively focusing along the North Pyrenean Zone, Earth-Science Reviews, 230, 104040, https://doi.org/10.1016/j.earscirev.2022.104040, 2022.

Bahroudi, A., and Koyi, H.: Effect of spatial distribution of Hormuz salt on deformation style in the Zagros fold and thrust belt: an analogue modelling approach. J. Geol. Soc. London, 160(5), 719-733, https://doi.org/10.1144/0016-764902-135,
590 2003.

Beaumont, C., Muñoz, J.A., Hamilton, J., and Fullsack, P.: Factors controlling the Alpine evolution of the central Pyrenees inferred from a comparison of observations and geodynamical models. J. Geophys. Res-Sol. Ea., 105(B4), 8121-8145, https://doi.org/10.1029/1999JB900390, 2000.

Bonini, M., Sani, F., and Antonielli, B.: Basin inversion and contractional reactivation of inherited normal faults: A review
595 based on previous and new experimental models. Tectonophysics, *522*, 55-88, https://doi.org/10.1016/j.tecto.2011.11.014, 2012.

Cadenas, P., Fernández-Viejo, G., Pulgar, J. A., Tugend, J., Manatschal, G., and Minshull, T.A.: Constraints imposed by rift inheritance on the compressional reactivation of a hyperextended margin: Mapping rift domains in the North Iberian margin and in the Cantabrian Mountains. Tectonics, 37(3), 758-785, https://doi.org/10.1002/2016TC004454, 2018.

600   Cadenas, P., Manatschal, G., and Fernández-Viejo, G.: Unravelling the architecture and evolution of the inverted multi-stage North Iberian-Bay of Biscay rift, Gondwana Res., 88, 67-87, https://doi.org/10.1016/j.gr.2020.06.026, 2020.

Cámara, P.: Inverted turtle salt anticlines in the eastern Basque-Cantabrian basin, Spain, Mar. Petrol. Geol., 104358, https://doi.org/10.1016/j.marpetgeo.2020.104358, 2020.

Cámara, P., and Flinch, J.F.: The southern Pyrenees: A salt-based fold-and-thrust belt, in: Permo-Triassic Salt Provinces of
605   Europe, North Africa and the Atlantic Margins, edited by: Soto, J.I., Flinch, J.F., and Tari, G., Elsevier, Amsterdam, Netherland, 395-415, https://doi.org/10.1016/B978-0-12-809417-4.00019-7, 2017.

Carola, E., Tavani, S., Ferrer, O., Granado, P., Quintà, A., Butillé, M., and Muñoz, J.A.: Along-strike extrusion at the transition between thin-and thick-skinned domains in the Pyrenean Orogen (northern Spain), in: Thick-skin-dominated orogens: From initial inversion to full accretion, edited by: Nemčok, M., Mora, A., Cosgrove, J.W. Geol. Soc., London,
610   Spec. Publ., 377(1), 119-140, https://doi.org/10.1144/SP377.3, 2013.

Carola, E., Muñoz, J.A., and Roca, E.: The transition from thick-skinned to thin-skinned tectonics in the Basque-Cantabrian Pyrenees: The Burgalesa Platform and surroundings. Int. J. Earth Sci., 104(8), 2215-2239, https://doi.org/10.1007/s00531-015-1177-z, 2015.

Carrera, N., Muñoz, J.A., Sàbat, F., Mon, R., and Roca, E.: The role of inversion tectonics in the structure of the Cordillera
615   Oriental (NW Argentinean Andes). J. Struct. Geol., 28(11), 1921-1932, https://doi.org/10.1016/j.jsg.2006.07.006, 2006.

Carrera, N. and Muñoz, J.A.: Thick-skinned tectonic style resulting from the inversion of previous structures in the southern Cordillera Oriental (NW Argentine Andes), in: Thick-skin-dominated orogens: From initial inversion to full accretion, edited by: Nemčok, M., Mora, A., Cosgrove, J.W., Geol. Soc., London, Spec. Publ., 377, 77–100, https://doi.org/10.1144/SP377.2, 2013.

620   Célini, N., Callot, J.-P., Ringenbach, J.-C. and Graham, R.: Jurassic Salt Tectonics in the SW Sub-Alpine Fold-and-Thrust Belt, Tectonics, 39(10), e2020TC006107, https://doi.org/10.1029/2020TC006107, 2020.

Chenin, P., Manatschal, G., Picazo, S., Müntener, O., Karner, G., Johnson, C., and Ulrich, M.: Influence of the architecture of magma-poor hyperextended rifted margins on orogens produced by the closure of narrow versus wide oceans, Geosphere, 13(2), 559-576, https://doi.org/10.1130/GES01363.1, 2017.

625   Chevrot, S., Sylvander, M., Díaz, J., Martin, R., Mouthereau, F., Manatschal, G., Masini, E., Calassou, S., Grimaud, F., Pauchet, H., and Ruiz, M.: The non-cylindrical crustal architecture of the Pyrenees, Sci Rep, 8, 9591, https://doi.org/10.1038/s41598-018-27889-x, 2018.

Cooper, M.A., Williams, G.D., de Graciansky, P.C., Murphy, R.W., Needham, T., de Paor, D., Stoneley, R., Todd, S.P., Turner, J.P. and Ziegler, P.A.: Inversion tectonics — a discussion, in: Inversion Tectonics, edited by: Copper, M.A., and
630   Williams, G.D., Geol. Soc., London, Spec. Publ., 44, 335-347, https://doi.org/10.1144/GSL.SP.1989.044.01.18, 1989.

Costa, E. and Vendeville, B.B.: Experimental insights on the geometry and kinematics of fold-and-thrust belt above weak, viscous evaporitic décollement. Journal of Structural Geology, 24, 1729–1739, 2002.

Cotton, J., and Koyi, H.: Modelling of thrust fronts above ductile and frictional décollements; examples from The Salt Range and Potwar Plateau, Pakistan. Geol. Soc. Am. Bull., 112(3), 351–363, https://doi.org/10.1130/0016-7606(2000)112<351:MOTFAD>2.0.CO;2, 2000.

Del Ventissette, C., Montanari, D., Bonini, M., and Sani, F.: Basin inversion and fault reactivation in laboratory experiments. J. Struct. Geol., 28, 2067-2083, https://doi.org/10.1016/j.jsg.2006.07.012, 2006.

Dell'Ertole, D., and Schellart, W.P.: The development of sheath folds in viscously stratified materials in simple shear conditions: An analogue approach. J. Struct. Geol., 6, 129-141, https://doi.org/10.1016/j.jsg.2013.09.002, 2013.

Dooley, T.P., and Hudec, M.R.: Extension and inversion of salt-bearing rift systems, Solid Earth, 11, 1187-1204, https://doi.org/10.5194/se-11-1187-2020, 2020.

Dooley, T., McClay, K.R., Hempton, M., and Smit, D.: Salt tectonics above complex basement extensional fault systems: results from analogue modelling, in: Petroleum Geology: North-West Europe and global perspectives – Proceedings of the 6th Petroleum Geology Conference, edited by: Doré, A.G., and Vining, B.A., 6 (1), 1631-1648, Geological Society, London, https://doi.org/10.1144/0061631, 2005.

Espina, R.G.: Extensión mesozoica y acortamiento alpino en el borde occidental de la Cuenca Vasco Cantábrica. Cad. Lab. Xeol. Laxe, 19, 137-150, 1994.

Espina, R.G.: Tectónica extensional en el borde occidental de la Cuenca Vasco- Cantábrica (Cordillera Cantábrica, NO de España). Geogaceta, 20(4), 890 – 892, 1996.

Ferrer, O., Roca, E., Benjumea, B., Munoz, J., Ellouz, N., and MARCONI, T.: The deep seismic reflection MARCONI-3 profile: Role of extensional Mesozoic structure during the Pyrenean contractional deformation at the eastern part of the Bay of Biscay, Marine and Petroleum Geology, 25, 714–730, 2008.

Ferrer, O., McClay, K.R., Sellier, N.C.: Influence of fault geometries and mechanical anisotropies on the growth and inversion of hanging-wall synclinal basins: insights from sandbox models and natural examples, in: The Geometry and Growth of Normal Faults, edited by: Child, C., Holdsworth, R.E., Jackson, C.A.L., Manzocchi, T., Walsh, J.J., Yieldings, G., Geol. Soc., London, Spec. Publ., 439, 487-509, https://doi.org/10.1144/SP439.8, 2016.

Ferrer, O., Carola, E., and McClay, K.: Structural control of inherited salt structures during inversion of domino basement-fault system from an analogue modelling approach. Solid Earth, submitted.

Ferrer, O., Carola, E., McClay, K., and Bufaliza, N.: Analogue modeling of domino-style extensional fault basement fault systems with precinematic salt. AAPG Bull., 107(1), 23-47, https://doi.org/10.1306/08072221188, 2023a.

Frasca, G., Manatschal, G., Cadenas, P., Miró, J., and Lescoutre, R.: A kinematic reconstruction of Iberia using intracontinental strike-slip corridors. Terra Nova, 573-581, https://doi.org/10.1111/ter.12549, 2021.

Gallastegui, J.: Estructura cortical de la cordillera y margen continental cantábricos: perfiles ESCI-N, Trabajos de Geología, 22(22), 3-234, https://doi.org/10.17811/tdg.22.2000.3-234, 2000.

665 Gallastegui, J., Pulgar, J. A., and Gallart, J.: Alpine tectonic wedging and crustal delamination in the Cantabrian Mountains (NW Spain), Solid Earth, 7, 1043–1057, https://doi.org/10.5194/se-7-1043-2016, 2016.

García de Cortázar, A., and Pujalte, V.: Litoestratigrafia y facies del Grupo Cabuérniga (Malm-Valanginiense inferior?) al S de Cantabria-NE de Palencia. Cuadernos de Geología Ibérica, 8, 5–21, 1982.

García-Senz, J., Pedrera, A., Ayala, C., Ruiz-Constán, A., Robador, A., and Rodríguez-Fernández, L.R.: Inversion of the
670 north Iberian hyperextended margin: the role of exhumed mantle indentation during continental collision, in: Fold and thrust belts: Structural style, evolution and exploration, edited by: Hammerstein, J.A., Di Cuia, R., Cottam, M.A., Zamora, G., Butler, R.W.H., Geol. Soc., London, Spec. Publ., 490, 177-198, https://doi.org/10.1144/SP490-2019-112, 2019.

Ghani, H., Zeilinger, G., Sobel, E.R., and, Heidarzadeh, G.: Structural variation within the Himalayan fold and thrust belt: A case study from the Kohat-Potwar Fold Thrust Belt of Pakistan. J. Struct. Geol., 116, 34–46,
675 https://doi.org/10.1016/j.jsg.2018.07.022, 2018.

Gómez, J.J., Goy, A., and Barrón, E.: Events around the Triassic–Jurassic boundary in northern and eastern Spain: a review. Palaeogeogr. Palaeocl., 244(1-4), 89-110, https://doi.org/10.1016/j.palaeo.2006.06.025, 2007.

Granado, P., Ferrer, O., Muñoz, J. A., Thöny, W., and Strauss, P.: Basin inversion in tectonic wedges: Insights from analogue modelling and the Alpine-Carpathian fold-and-thrust belt. Tectonophysics, 703-704(C), 50–68,
680 https://doi.org/10.1016/j.tecto.2017.02.022, 2017.

Granado, P., Roca, E., Strauss, P., Pelz, K., and Munoz, J.A.: Structural styles in fold-and-thrust belts involving early salt structures: The Northern Calcareous Alps (Austria). Geology, 47(1), 51–54, https://doi.org/10.1130/G45281.1, 2018.

Hubbert, M.K.: Mechanical basis for certain familiar geologic structures. Geol. Soc. Am. Bull., 62(4), 355-372, https://doi.org/10.1130/0016-7606(1951)62[355:MBFCFG]2.0.CO;2, 1951.

685 Hardy, S., McClay, K., and Muñoz, J.A.: Deformation and fault activity in space and time in high-resolution numerical models of doubly vergent thrust wedges, Marine and Petroleum Geology, 26, 232–248, https://doi.org/10.1016/j.marpetgeo.2007.12.003, 2009.

Iaffa, D.N., Sàbat, F., Bello, D., Ferrer, O., Monn, R., and Gutierrez, A.A.: Tectonic inversion in a segmented foreland basin from extensional to piggy back settings: The Tucumán Basin in NW Argentina. J. S. Am. Earth Sci., 31(4), 457-474,
690 https://doi.org/10.1016/j.jsames.2011.02.009, 2011a.

Iaffa, D.N., Sàbat, F., Muñoz, J.A., Mon, R., and Gutierrez, A.A.: The role of inherited structures in a foreland basin evolution. The Metán Basin in NW Argentina. J. Struct. Geol., 33(12), 1816-1828, https://doi.org/10.1016/j.jsg.2011.09.005, 2011b.

Jackson, M.P., Vendeville, B.C., and Schultz-Ela, D.D.: Structural dynamics of salt systems. Annu. Rev. Earth Pl. Sc., 22(1),
695 93-117. https://doi.org/10.1146/annurev.ea.22.050194.000521, 1994.

Jaumé, S.C., and Lillie, R.J.: Mechanics of the Salt Range-Potwar Plateau, Pakistan: a fold-and-thrust belt underlain by evaporites, Tectonics, 7(1), 57–71, https://doi.org/ Mechanics of the Salt Range-Potwar Plateau 10.1029/TC007i001p00057, 1988.

Jourdon, A., Mouthereau, F., Pourhiet, L. L. & Callot, J.-P.: Topographic and Tectonic Evolution of Mountain Belts Controlled by Salt Thickness and Rift Architecture. Tectonics 39, e2019TC005903. https://doi.org/10.1029/2019TC005903, 2020.

Lagabrielle, Y., Asti, R., Duretz, T., Clerc, C., Fourcade, S., Teixell, A., Labaume, P, Corre, B., and Saspiturry, N.: A review of cretaceous smooth-slopes extensional basins along the Iberia-Eurasia plate boundary: How pre-rift salt controls the modes of continental rifting and mantle exhumation, Earth-Sci. Rev., 201, 103071, https://doi.org/10.1016/j.earscirev.2019.103071, 2020.

Lescoutre, R., and Manatschal, G.: Role of rift-inheritance and segmentation for orogenic evolution: example from the Pyrenean-Cantabrian system, B. Soc. Geol. Fr., 191(1), 18, https://doi.org/10.1051/bsgf/2020021, 2020.

Lescoutre, R., Manatschal, G., and Muñoz, J.A.: Nature, Origin, and Evolution of the Pyrenean-Cantabrian Junction. Tectonics, 40(5), e2020TC006134, https://doi.org/10.1029/2020TC006134, 2021.

López-Gómez, J., Martín-González, F., Heredia, N., Horra, R. de la, Barrenechea, J. F., Cadenas, P., Juncal, M., Diez, J. B., Borruel-Abadía, V., Pedreira, D., García-Sansegundo, J., Farias, P., Galé, C., Lago, M., Ubide, T., Fernández-Viejo, G., and Gand, G.: New lithostratigraphy for the Cantabrian Mountains: A common tectono-stratigraphic evolution for the onset of the Alpine cycle in the W Pyrenean realm, N Spain, Earth-sci Rev, 188, 249–271, https://doi.org/10.1016/j.earscirev.2018.11.008, 2019.

Liu Huiqi, McClay, K.R. & Powell, D.: Physical models of thrust wedges, in: Thrust Tectonics, edited by McClay, K.R., Chapman and Hall, London, 71–81, 1992.

Manatschal, G., Chenin, P., Lescoutre, R., Miró, J., Cadenas, P., Saspiturry, N., Masini, E., Chevrot, S., Ford, M., Jolivet, L., Mouthereau, F., Thinon, I., Issautier, B. and Calassou, S.: The role of inheritance in forming rifts and rifted margins and building collisional orogens: a Biscay-Pyrenean perspective. B. Soc. Geol. Fr., 192 (1), 55, https://doi.org/10.1051/bsgf/2021042, 2021.

Mandl, G., De Jong, L.N.J., and Maltha, A.: Shear zones in granular material. Rock Mech., 9(2-3), 95-144, https://doi.org/10.1007/BF01237876, 1977.

Marrett, R. and Aranda-García, M.: Regional structure of the Sierra Madre Oriental fold-thrust belt, Mexico, in R. Marrett, ed., Genesis and controls of reservoir-scale carbonate deformation, Monterrey salient, Mexico: Bureau of Economic Geology, Austin, Guidebook 28, 31-55, 2001.

Martínez Catalán, J.R., Arenas, R., García, F.D., Cuadra, P.G., Gómez-Barreiro, J., Abati, J., Castiñeiras, P., Fernández, J., Sánchez, S., Andonaegui, P., González, E., Díez, A., Rubio, F.J., and Valle, B.: Space and time in the tectonic evolution of the northwestern Iberian Massif: Implications for the Variscan belt, in: 4-D Framework of Continental Crust, edited by: Hatcher Jr., R.D., Carlson, M.P.; McBride, J.H., and Martínez-Catalán, J.R., Geol. Soc. Am. Mem., 200, 403–423, https://doi.org/10.1130/2007.1200(21), 2007.

Matte, P.: Accretionary history and crustal evolution of the Variscan belt in Western Europe, Tectonophysics, 196(3–4), 309–337, https://doi.org/10.1016/0040-1951(91)90328-P, 1991.

Mazur, S., Scheck-Wenderoth, M., and Krzywiec, P.: Different modes of the Late Cretaceous–Early Tertiary inversion in the North German and Polish basins, Int J Earth Sci (Geol Rundsch), 94, 782–798, https://doi.org/10.1007/s00531-005-0016-z, 2005.

McClay, K.R.: Analogue models of inversion tectonics, in: Inversion Tectonics, edited by: Cooper, M.A., and Williams, G.D., Geol. Soc., London, Spec. Publ., 44, 41-59, https://doi.org/10.1144/GSL.SP.1989.044.01.04, 1989.

McClay, K.R., and Buchanan, P.G.: Thrust faults in inverted extensional basins, in: Thrust tectonics, edited by: McClay, K.R., 93-104, Springer, Dordrecht, Netherland, https://doi.org/10.1007/978-94-011-3066-0_8, 1992.

McClay, K.R., and White, M.J.: Analogue modelling of orthogonal and oblique rifting, Mar. Petrol. Geol., 12(2), 137-151, https://doi.org/10.1016/0264-8172(95)92835-K, 1995.

Miró, J., Muñoz, J.A., Manatschal, G., and Roca, E.: The Basque–Cantabrian Pyrenees: report of data analysis. B. Soc. Geol. Fr., 191(1), 22, https://doi.org/10.1051/bsgf/2020024, 2020.

Miró, J., Manatschal, G., Cadenas, P., and Muñoz, J.A.: Reactivation of a hyperextended rift system: the Basque-Cantabrian Pyrenees case, Basin Res., 33(6), 3077-3101, https://doi.org/10.1111/bre.12595, 2021.

Molinaro, M., Leturmy, P., Guezou, J.C., Frizon de Lamotte, D., and Eshraghi, S.A.: The structure and kinematics of the southeastern Zagros fold-thrust belt, Iran: From thin-skinned to thick-skinned tectonics, Tectonics, 24(3), TC3007, https://doi.org/10.1029/2004TC001633, 2005.

Mouthereau, F., Tensi, J., Bellahsen, N., Lacombe, O., De Boisgrollier, T., and Kargar, S.: Tertiary sequence of deformation in a thin-skinned/thick-skinned collision belt: The Zagros Folded Belt (Fars, Iran). Tectonics, 26, TC5006, doi:10.1029/2007TC002098, 2007.

Muñoz, J.A.: Evolution of a continental collision belt: ECORS-Pyrenees crustal balanced cross-section, in: Thrust tectonics, edited by: McClay, K.R., 235-246, Springer, Dordrecht, Netherland, https://doi.org/10.1007/978-94-011-3066-0_21, 1992.

Muñoz, J., Beamud, E., Fernández, O., Arbués, P., Dinarès-Turell, J., and Poblet, J.: The Ainsa Fold and thrust oblique zone of the central Pyrenees: Kinematics of a curved contractional system from paleomagnetic and structural data, Tectonics, 32, 1142–1175, https://doi.org/10.1002/tect.20070, 2013.

Muñoz, J.A., Mencos, J., Roca, E., Carrera, N., Gratacós, Ò., Ferrer, O., and Fernández, O.: The structure of the South-Central-Pyrenean fold and thrust belt as constrained by subsurface data, Geol. Acta, 16(4), 439-460, https://doi.org/10.1344/GeologicaActa2018.16.4.7, 2018.

Muñoz, J.A.: Alpine Orogeny: Deformation and Structure in the Northern Iberian Margin (Pyrenees sl), in: The Geology of Iberia: A Geodynamic Approach, Volume 5: Active processes: seismicity, active faulting and relief, edited by: Quesada, C., and Oliveira, J.T., 433-451, Springer, Amsterdam, Netherlands, https://doi.org/ 10.1007/978-3-030-11295-0_9, 2019.

Pedreira, D., Afonso, J.C., Pulgar, J.A., Gallastegui, J., Carballo, A., Fernández, M., García-Castellanos, D., Jiménez-Munt, I., Semprich, J. and García-Moreno, O.: Geophysical-petrological modeling of the lithosphere beneath the Cantabrian Mountains and the North-Iberian margin: Geodynamic implications. Lithos, 230, 46-68, https://doi.org/10.1016/j.lithos.2015.04.018, 2015.

Pedrera, A., García-Senz, J., Ayala, C., Ruiz-Constán, A., Rodríguez-Fernández, L.R., Robador, A., and González Menéndez, L.: Reconstruction of the exhumed mantle across the North Iberian Margin by crustal-scale 3-D gravity inversion and geological cross section. Tectonics, 36(12), 3155-3177, https://doi.org/10.1002/2017TC004716, 2017.

770 Pedrera, A., García-Senz, J., Peropadre, C., Robador, A., López-Mir, B., Díaz-Alvarado, J., and Rodríguez-Fernández, L.R.: The Getxo crustal-scale cross-section: Testing tectonic models in the Bay of Biscay-Pyrenean rift system. Earth-Sci. Rev., 212, 103429, https://doi.org/10.1016/j.eartscirev.2020.103429, 2020.

Pinto, L., Muñoz, C., Nalpas, T., and Charrier, R.: Role of sedimentation during basin inversion in analogue modelling, J. Struct. Geol., 32(4), 554-565, https://doi.org/10.1016/j.jsg.2010.03.001, 2010.

775 Pulgar, J.A., Alonso, J.L., Espina, R.G., and Marín, J.A.: La deformación alpina en el basamento varisco de la Zona Cantábrica, Trabajos De Geología, 21(21), 283–295, https://doi.org/10.17811/tdg.21.1999.283-295, 1999.

Quintana, L., Pulgar, J.A., and Alonso, J.L.: Displacement transfer from borders to interior of a plate: A crustal transect of Iberia, Tectonophysics, 663, 378-398, https://doi.org/10.1016/j.tecto.2015.08.046, 2015.

Quirk, D.G., and Pilcher, R.S.: Flip-flop salt tectonics, in: Salt tectonics, sediments and prospectivity, edited by: Alsop, G.I., 780 Archer, S.G., Hartley, A.J., Grant, N.T., Hodgkinson, R., Geol. Soc., London, Spec. Publ., 363, 245-264. https://doi.org/10.1144/SP363.11, 2012.

Riba, O., Jurado, M.J.: Reflexiones sobre la geologia de la parte occidental de la Depresión del Ebro. Acta Geológica Hispánica, Libro Homenaje a Oriol Riba Arderiu, 27(1/2), 177–193, 1992.

Roca, E., Muñoz, J.A., Ferrer, O., and Ellouz, N.: The role of the Bay of Biscay Mesozoic extensional structure in the 785 configuration of the Pyrenean orogen: Constraints from the MARCONI deep seismic reflection survey, Tectonics, 30(2). https://doi.org/10.1029/2010TC002735, 2011.

Roest, W.R., and Srivastava, S.P.: Kinematics of the plate boundaries between Eurasia, Iberia, and Africa in the North Atlantic from the Late Cretaceous to the present, Geology, 19(6), 613-616, https://doi.org/10.1130/0091-7613(1991)019<0613:KOTPBB>2.3.CO;2, 1991.

790 Roma, M., Ferrer, O., Roca, E., Pla, O., Escosa, F.O., and Butillé, M.: Formation and inversion of salt-detached ramp-syncline basins. Results from analog modeling and application to the Columbrets Basin (Western Mediterranean), Tectonophysics, 745, 214-228, https://doi.org/10.1016/j.tecto.2018.08.012, 2018a.

Roma, M., Vidal-Royo, O., McClay, K., Ferrer, O., and Muñoz, J.A.: Tectonic inversion of salt-detached ramp-syncline basins as illustrated by analog modeling and kinematic restoration, Interpretation, 6(1), T127-T144, 795 https://doi.org/10.1190/INT-2017-0073.1, 2018b.

Rowan, M.G.: Passive-margin salt basins: Hyperextension, evaporite deposition, and salt tectonics, Basin Res., 26(1), 154-182, https://doi.org/10.1111/bre.12043, 2014.

Rowan, M.G., and Giles, K.A.: Passive versus active salt diapirism, AAPG Bull., 105, 53-63, https://doi.org/10.1306/05212020001, 2020.

800 Sani, F., Del Ventisette, C., Montanari, D., Bendkik, A., Chenakeb, M.: Structural evolution of the Rides Prerifaines (Morocco): structural and seismic interpretation and analogue modelling experiments, Int. J. Earth Sci. (Geol. Rundsch.), 96, 685-706, htpps://doi.org/10.1007/s00531-006-0118-2, 2007.

Saspiturry, N., Allanic, C., Razin, P., Issautier, B., Baudin, T., Lasseur, E., Serrano, O., and Leleu, S.: Closure of a hyperextended system in an orogenic lithospheric pop-up, Western Pyrenees: The role of mantle buttressing and rift
805 structural inheritance, Terra Nova, 32(4), 253-260, https://doi.org/10.1111/ter.12457, 2020.

Schellart, W.P.: Shear test results for cohesion and friction coefficients for different granular materials: scaling implications for their usage in analogue modelling, Tectonophysics, 324(1-2), 1-16, https://doi.org/10.1016/S0040-1951(00)00111-6, 2000.

Sherkati, S., Letouzey, J. and Lamotte, D. F. de: Central Zagros fold-thrust belt (Iran): New insights from seismic data, field
810 observation, and sandbox modelling. Tectonics, 25, TC4007, doi:10.1029/2004TC001766, 2006.

Tavani, S., Carola, E., Granado, P., Quintà, A., and Muñoz, J.A.: Transpressive inversion of a Mesozoic extensional forced fold system with an intermediate décollement level in the Basque-Cantabrian Basin (Spain), Tectonics, 32(2), 146-158, https://doi.org/10.1002/tect.20019, 2013.

Tavani, S., Bertok, C., Granado, P., Piana, F., Salas, R., Vigna, B., and Muñoz, J.A.: The Iberia-Eurasia plate boundary east
815 of the Pyrenees, Earth-Sci. Rev., 187, 314-337, https://doi.org/10.1016/j.earscirev.2018.10.008, 2018.

Teixell, A.: Crustal structure and orogenic material budget in the west central Pyrenees, Tectonics, 17(3), 395-406, https://doi.org/10.1029/98TC00561, 1998.

Tugend, J., Manatschal, G., Kusznir, N.J., Masini, E., Mohn, G., and Thinon, I.: Formation and deformation of hyperextended rift systems: Insights from rift domain mapping in the Bay of Biscay-Pyrenees, Tectonics, 33(7), 1239-1276,
820 https://doi.org/10.1002/2014TC003529, 2014.

Tugend, J., Manatschal, G., and Kusznir, N.J.: Spatial and temporal evolution of hyperextended rift systems: Implication for the nature, kinematics, and timing of the Iberian-European plate boundary, Geology, 43(1), 15-18, https://doi.org/10.1130/G36072.1, 2015.

Vendeville, B.C., and Jackson, M.P.: The rise of diapirs during thin-skinned extension, Mar. Petrol. Geol., 9(4), 331-354,
825 https://doi.org/10.1016/0264-8172(92)90047-I, 1992a.

Vendeville, B.C. and Jackson, M.P.A.: The fall of diapirs during thin-skinned extension, Mar. Petrol. Geol., 9 (4), 354-371, https://doi.org/10.1016/0264-8172(92)90048-J, 1992b.

Weijermars, R.: Flow behaviour and physical chemistry of bouncing putties and related polymers in view of tectonic laboratory applications, Tectonophysics, 124(3-4), 325-358, https://doi.org/10.1016/0040-1951(86)90208-8, 1986.
830 Wilson, Elizabeth P.; Granado, P.; Santolaria, P.; Ferrer, O.; and Muñoz, J.A.: Inversion of transfer zones in salt-bearing systems: Insights from analogue modelling. Solid Earth, submitted.

Withjack, M.O., and Callaway, S.: Active normal faulting beneath a salt layer: an experimental study of deformation patterns in the cover sequence, AAPG Bull., 84(5), 627-651, https://doi.org/10.1306/C9EBCE73-1735-11D7-8645000102C1865D, 2000.

835 Wolf, S. G., Huismans, R. S., Munoz, J. A., Curry, M. E., and Beek, P. van der: Growth of Collisional Orogens From Small and Cold to Large and Hot—Inferences From Geodynamic Models, J. Geophys. Res. Solid Earth, 126, e2020JB021168, https://doi.org/10.1029/2020jb021168, 2021.

Wu, J.E., McClay, K., Whitehouse, P., and Dooley, T.: 4D analogue modelling of transtensional pull-apart basins, Mar. Petrol. Geol., 26(8), 1608-1623, https://doi.org/10.1016/j.marpetgeo.2008.06.007, 2009.

840
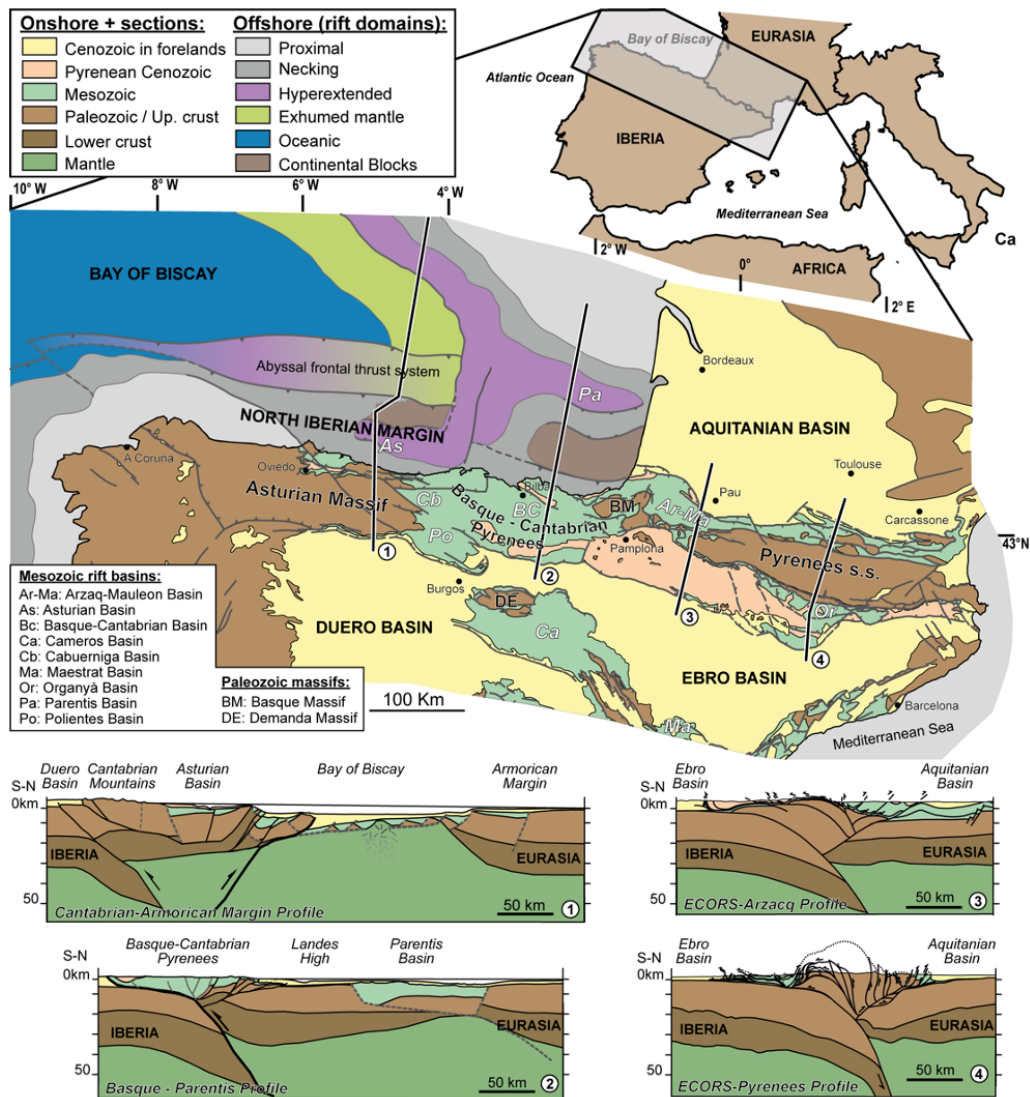
Figure 1: Structural map of the Pyrenean Orogen and surrounding areas with crustal cross-sections depicting the main along-strike structural changes. Rift domains are also mapped offshore. 1) Asturian Massif – Armorican Margin (Cadenas et al., 2018); 2) Basque – Cantabrian Pyrenees – Parentis (Ferrer et al., 2008 and Roca et al. 2011); 3) ECORS-Arzaq (Teixell, 1998); and 4) ECORS-Pyrenees (Muñoz, 1992).
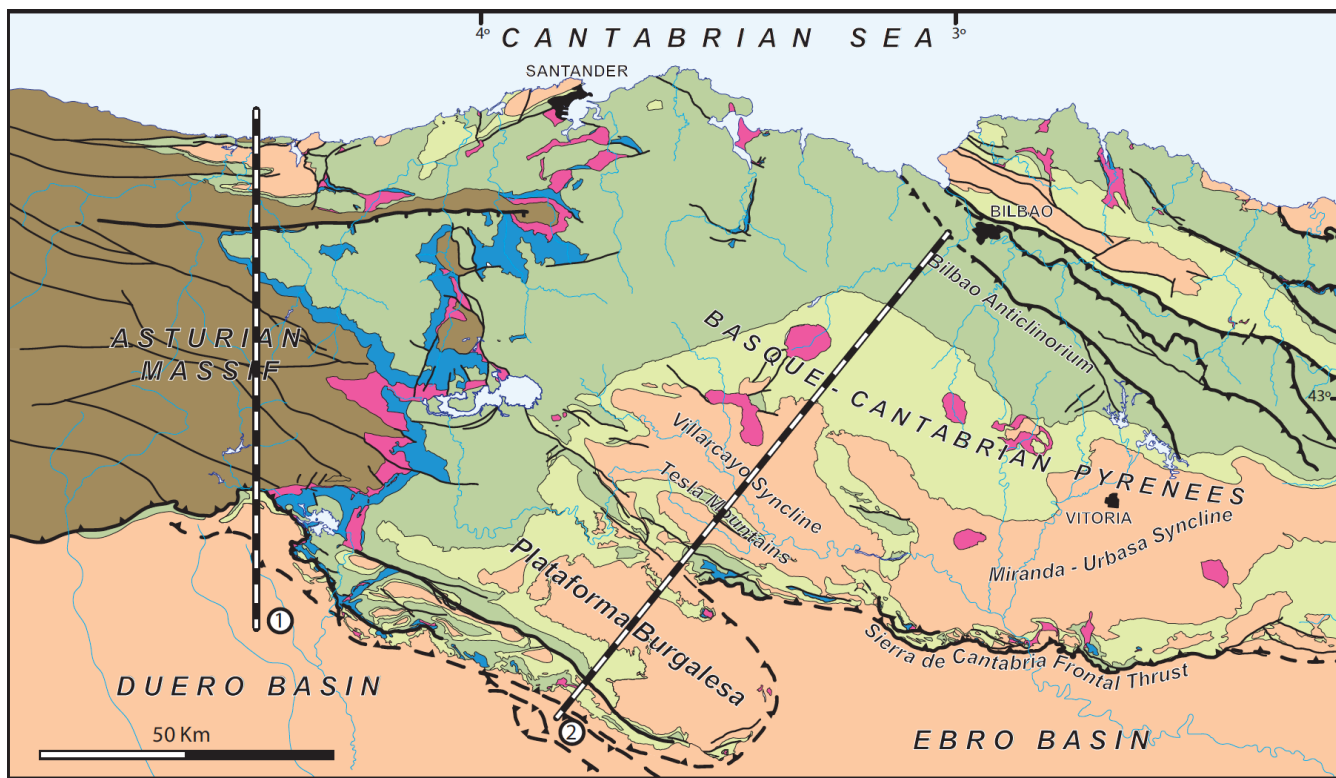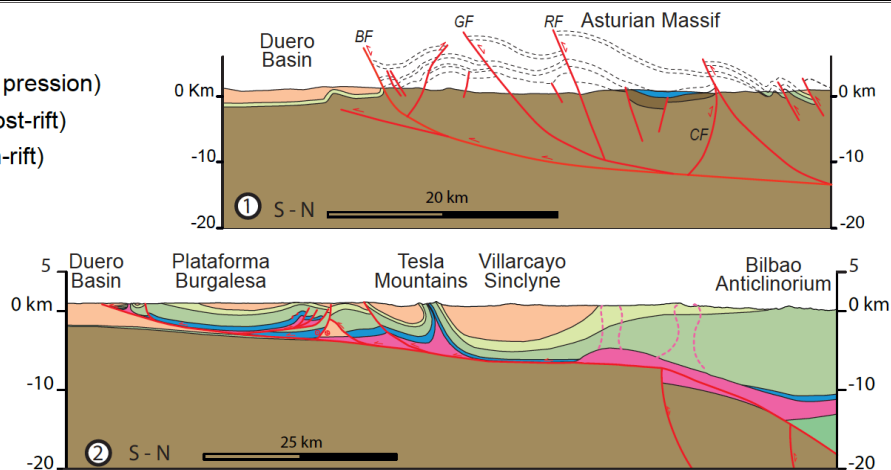
Figure 2: Tectonostratigraphic map of the Basque – Cantabrian Pyrenees – Asturian Massif junction (modified from Miró et al., 2021), and geological cross-section showing the along-strike variability of the structural style, from thick-skinned to the West to thin-skinned to the East. Cross-section 1 from Espina (1996) and cross-section 2 from Miró et al., 2021. BF: Becerril Fault, GF: Golobar Fault, RF: Rumaceo Fault, CF: Cabuérniga Fault.

860
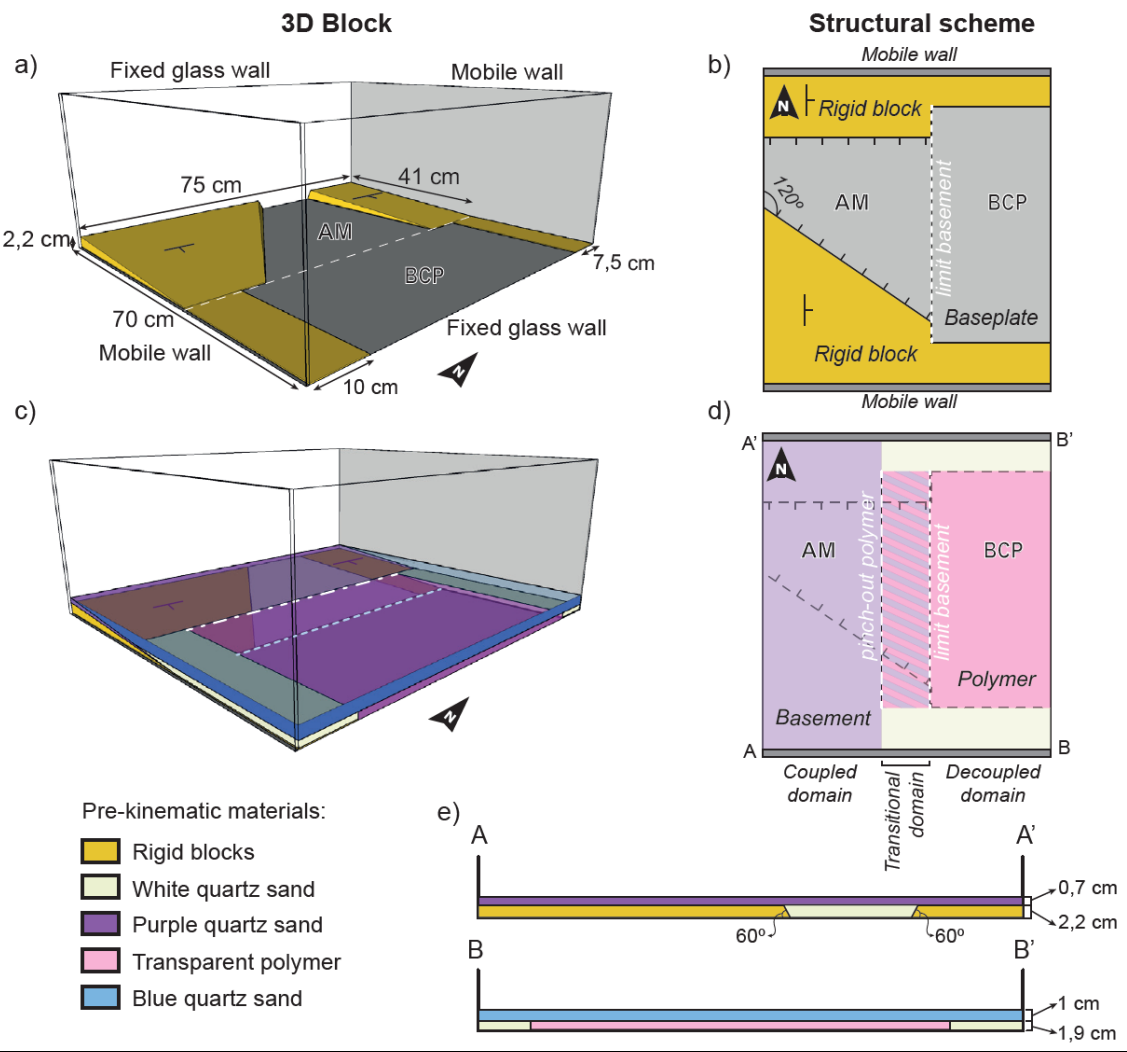
Figure 3: 3D blocks (left) and overhead sketches (right) of the experimental setup. a) 3D block showing the distribution of the rigid blocks at the base of the model. b) Overhead sketch of the previous 3D block. c) Final experimental configuration before extensional deformation showing the distribution of the different layers. The limit of the basement and the pinch out of the polymer are also indicated (see Figure 3d for legend). d) Overhead sketch showing the distribution of basement sand and polymer indicating the overlapping area and the boundaries of both units, which defines the different structural domains. e) Cross-sections of the coupled and decoupled domains prior to extension. See Figure 3d for location. AM (Asturian Massif) and BCP (Basque - Cantabrian Pyrenees) represent the modeled analogue domains in nature.
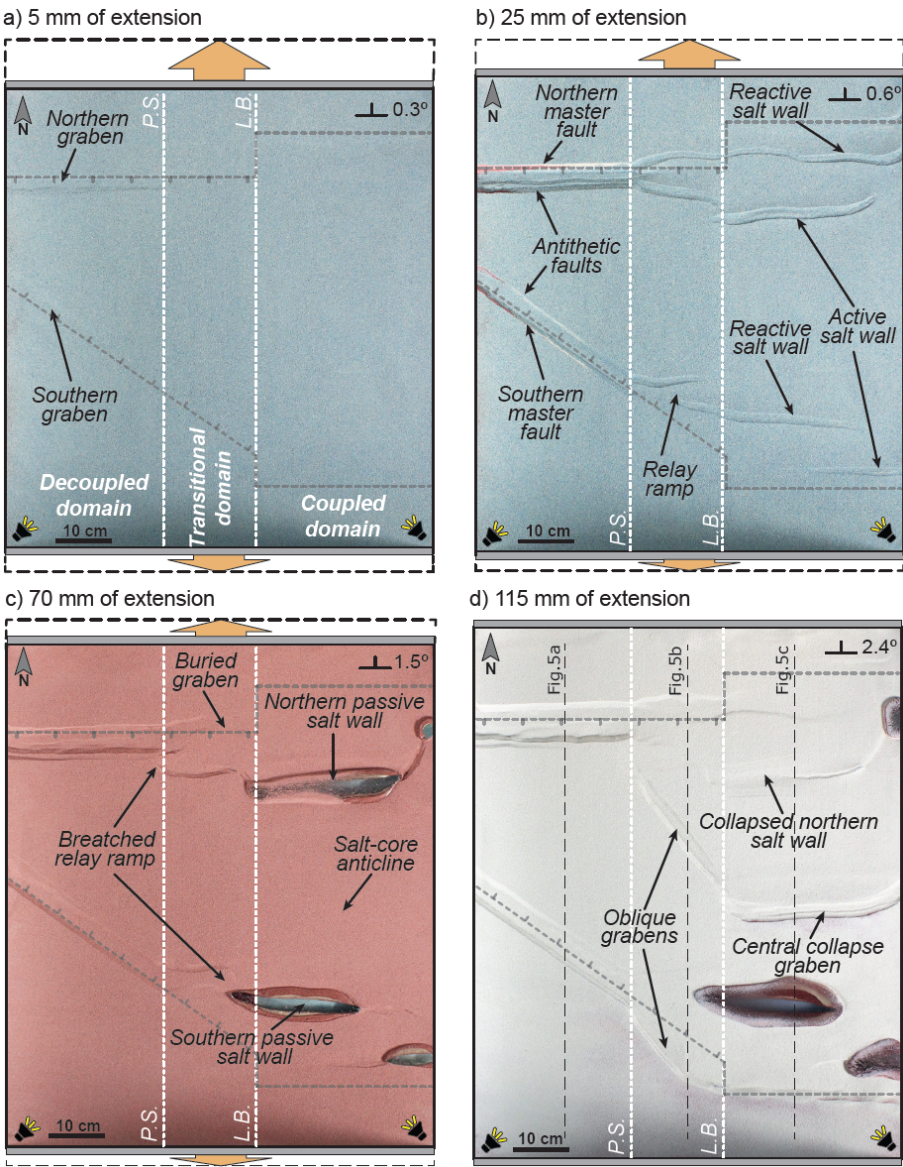
865

Figure 4: Overhead evolution of Model-1 during extension. Illumination comes from the left. The shadow areas are surface-breaching faults dipping to the right (North) and the illuminated ones are surface-breaching faults dipping to the left (South). The position of the basement rigid blocks is shown in grey dotted lines, and the polymer pinch out (P.S.) and the limit of basement blocks (L.B.) in white dotted lines. a) Overhead view after 5 mm of extension. b) Overhead view after 25 mm of extension. c) Overhead view after 70 mm of extension. d) Overhead view after 115 mm of extension. The external dashed reference rectangle corresponds to the dimensions of the experiment after 115mm of extension (step d) to show the movement of the two walls through time. The northern wall moved at a higher velocity than the southern one as represented by the arrows. 8 different layers (alternating red and white sand) were added during the extension.
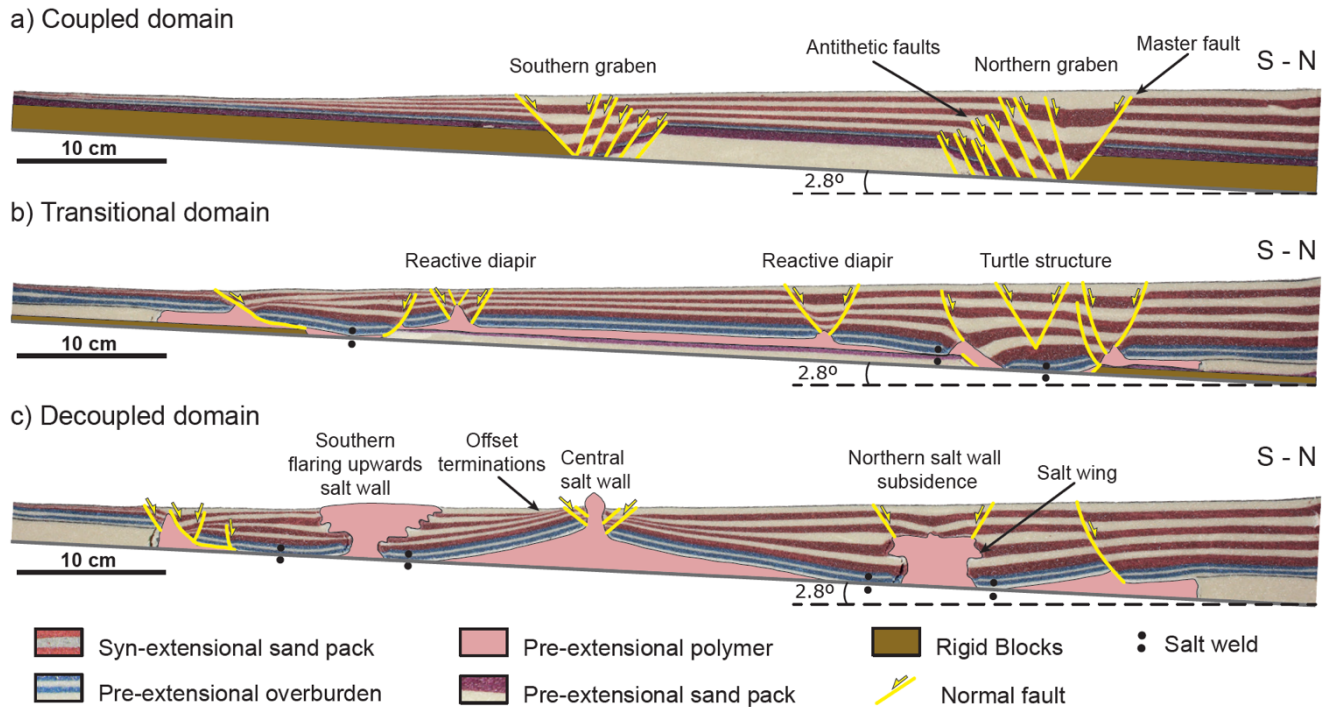
Figure 5: Cross-sections at the end of the extensional deformation (127 mm) across the different structural domains of Model-1. a) Coupled domain; b) Transitional domain; c) Decoupled domain. See Figure 4d for location. Before the sedimentation of each syn-extensional layer, the rig was tilted 0.35°northwards to simulate the progressive tilting of an extensional rifted margin reaching a regional dip of 2.8° at the end of the extensional phase.

890
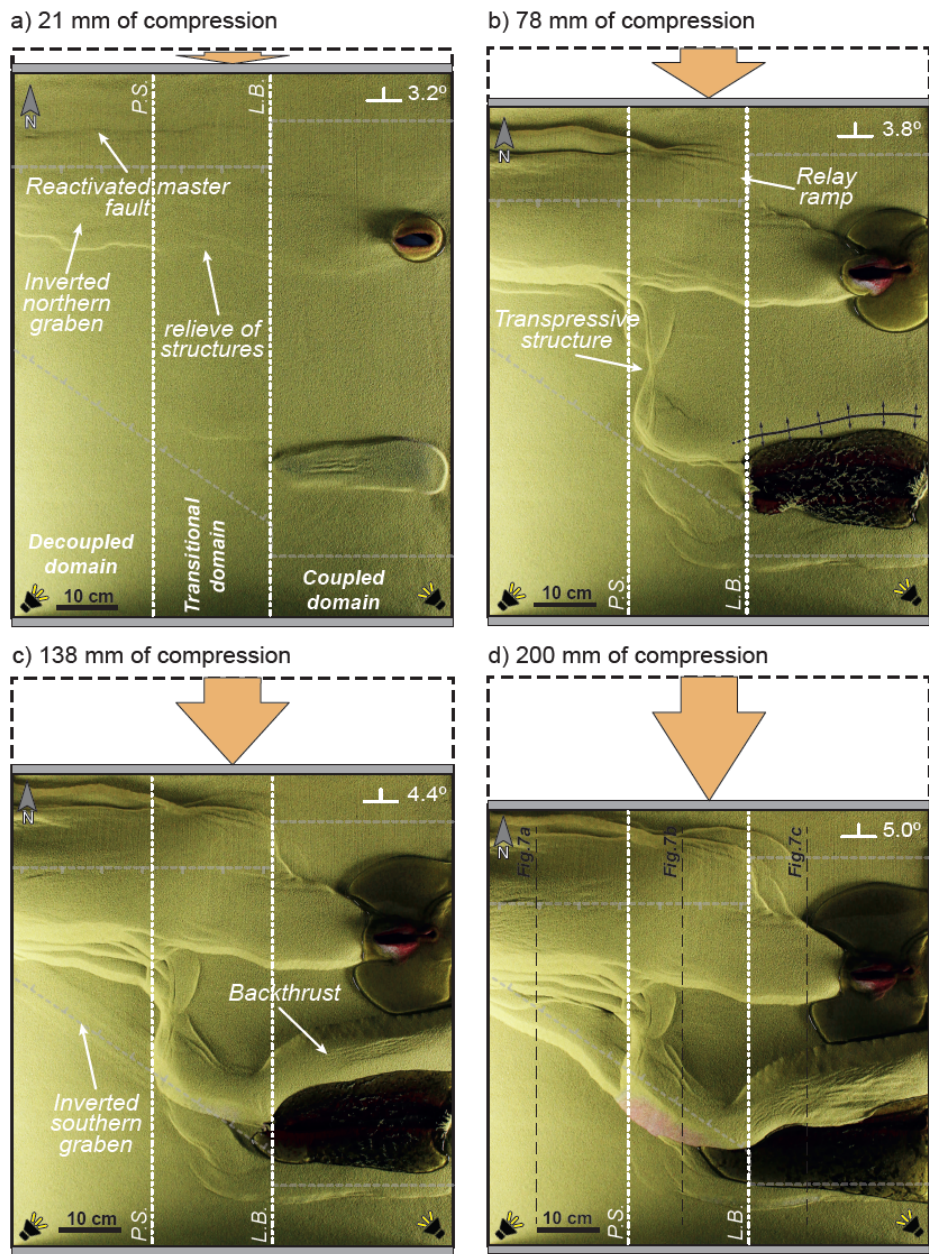
Figure 6: Overhead pictures showing the evolution of Model-2. Illumination comes from the left. The position of the basement rigid blocks is shown in grey dotted lines and the pinch out of the polymer (P.S.) and the limit of basement blocks (L.B.) in white dotted lines. a) Overhead view after 21 mm of shortening. b) Overhead view after 78 mm of shortening. c) Overhead view after 138 mm of shortening. d) Overhead view at the end of the experiment (200 mm shortening). No syn-tectonic sedimentation was performed during the compressional phase of this experiment.
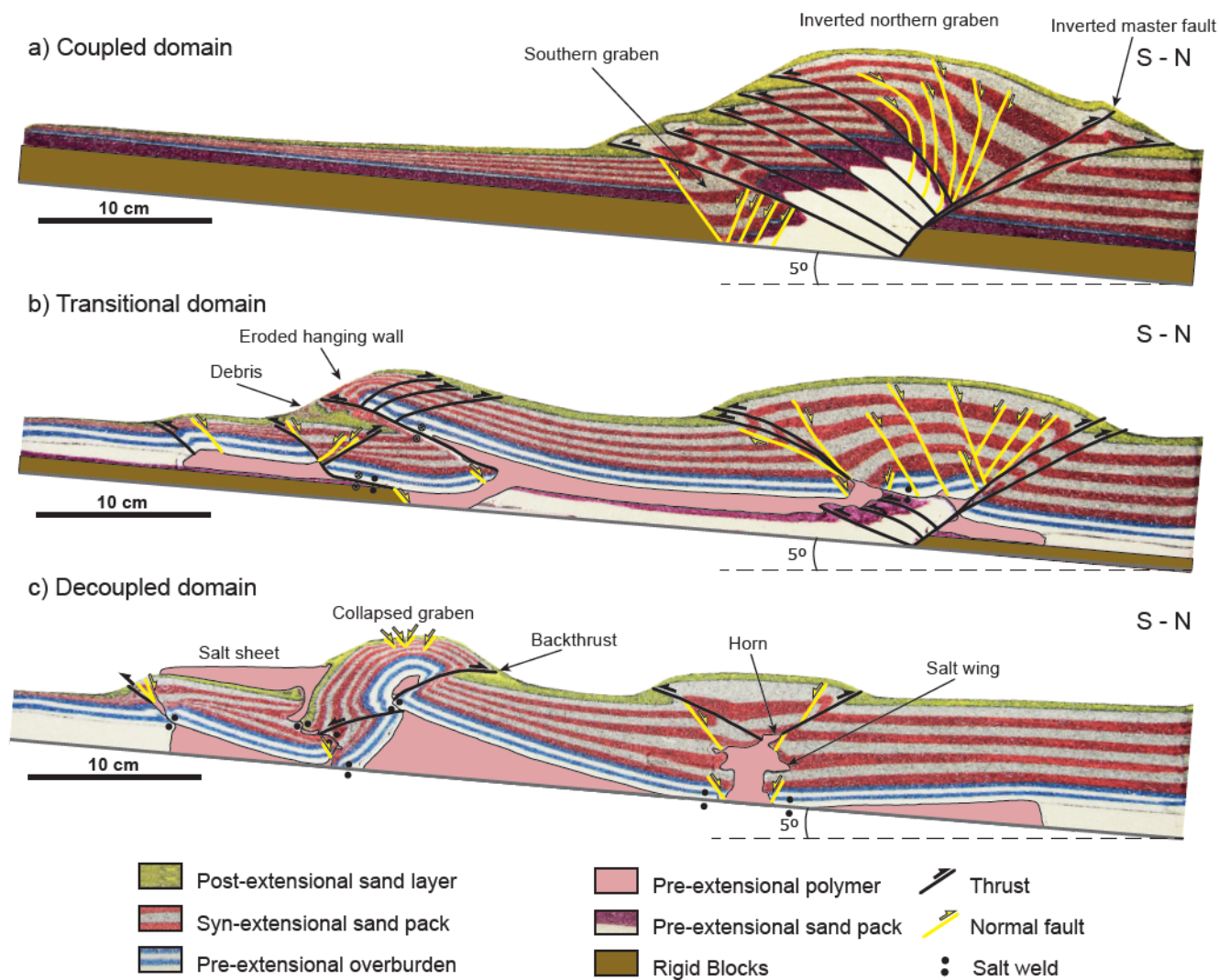
Figure 7: Cross-sections at the end of the Model-2 (after 200 mm of shortening) showing the structural style at the different domains. a) Coupled domain; b) Transitional domain; c) Decoupled domain. See figure 6d for location. The rig was tilted to the north up to additional 2.2° to simulate the orogenic flexure of the Basque – Cantabrian Pyrenees.
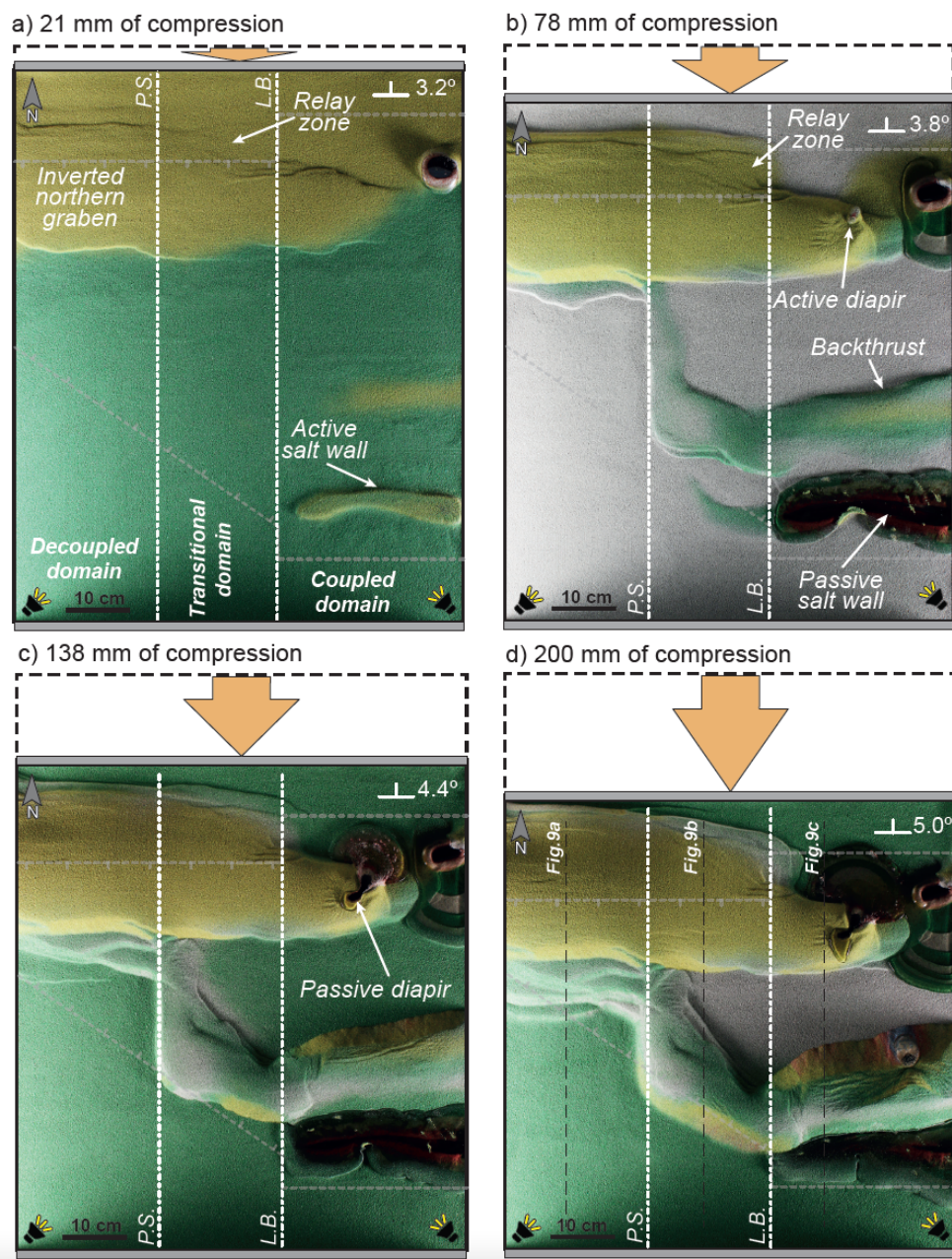
Figure 8: Overhead pictures showing the evolution of Model-3. Illumination comes from the left. The position of the basement rigid blocks is shown in grey dotted lines and the pinch out of the polymer (P.S.) and the limit of basement blocks (L.B.) in white dotted lines. a) Overhead view after 21 mm of shortening. b) Overhead view after 78 mm of shortening. c) Overhead view after 138 mm of shortening. d) Overhead view at the end of the experiment (200 mm shortening). Syn-orogenic sedimentation has been performed during the compressional phase of this experiment by adding alternating green and white sand layers every 3 hours.

915
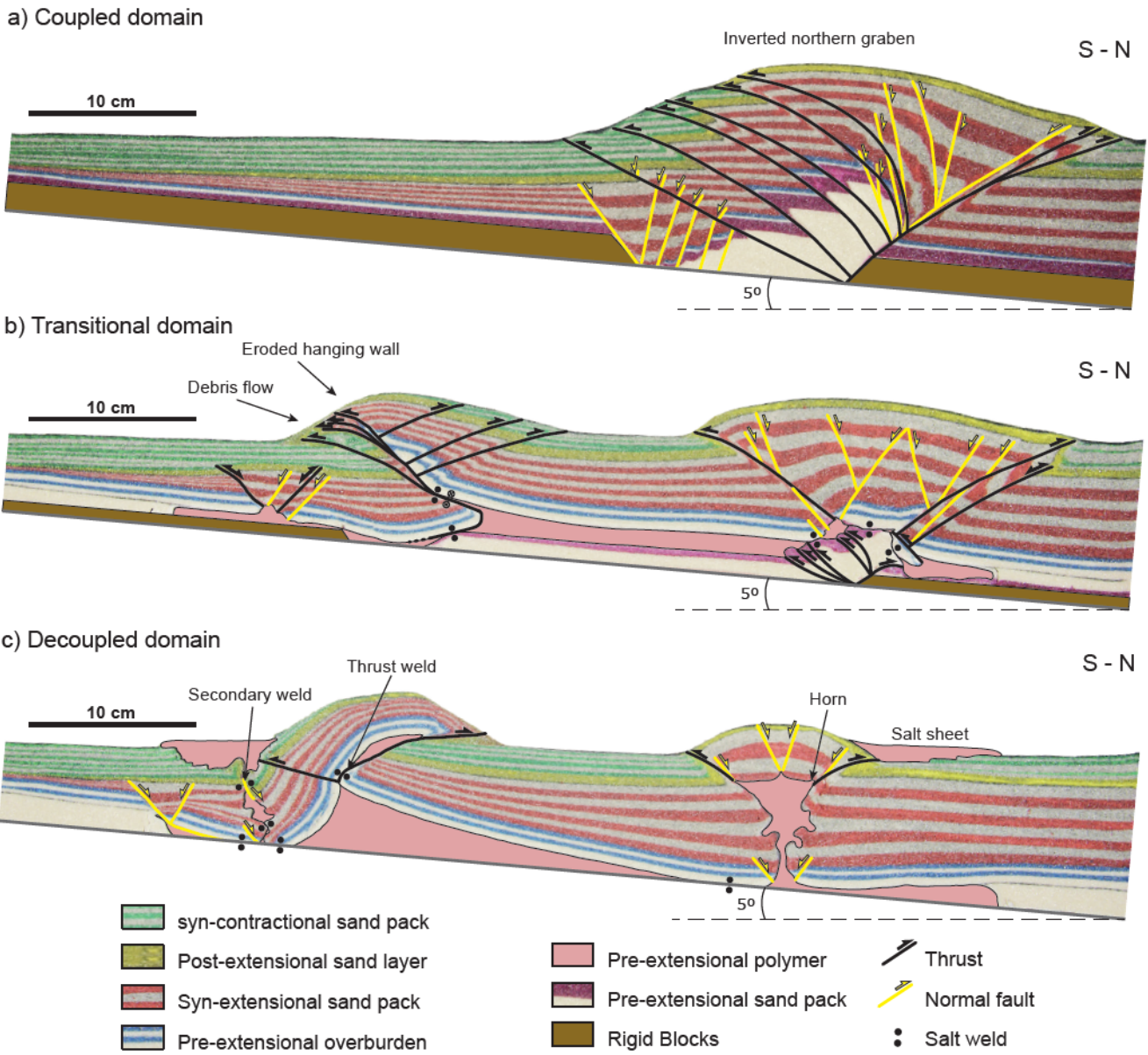
Figure 9: Cross-sections at the end of the Model-3 (after 200 mm of shortening) showing the structural style at the different domains. a) Coupled domain; b) Transitional domain; c) Decoupled domain. See figure 8d for location. After the deposition of each syn-compressional sand layer, the rig was tilted 0.2° to the north up to additional 2.2° to simulate the orogenic flexure of the Basque – Cantabrian Pyrenees.

925
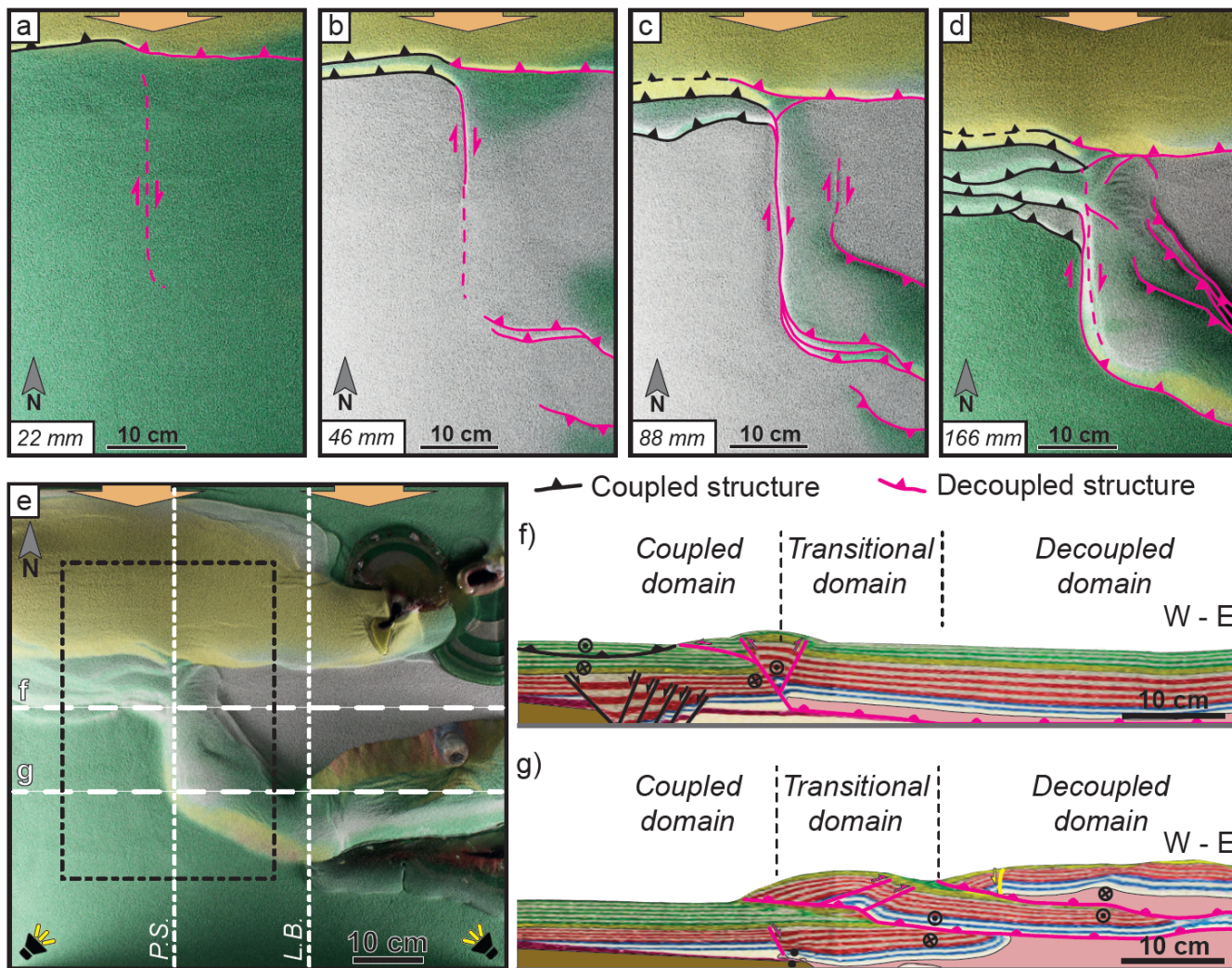
Figure 10: a to d) Detail of the overhead evolution of the transitional domain in Model-3 after 22, 46, 88, and 166 mm of shortening respectively. e) Overhead view at the end of the Model-3 (after 200 mm of shortening). The black square indicates the location of Figure 10d. f and g) W-E cross-sections built from a 3D voxel showing the structural style of the transitional domain (see location in Figure 10e).

930
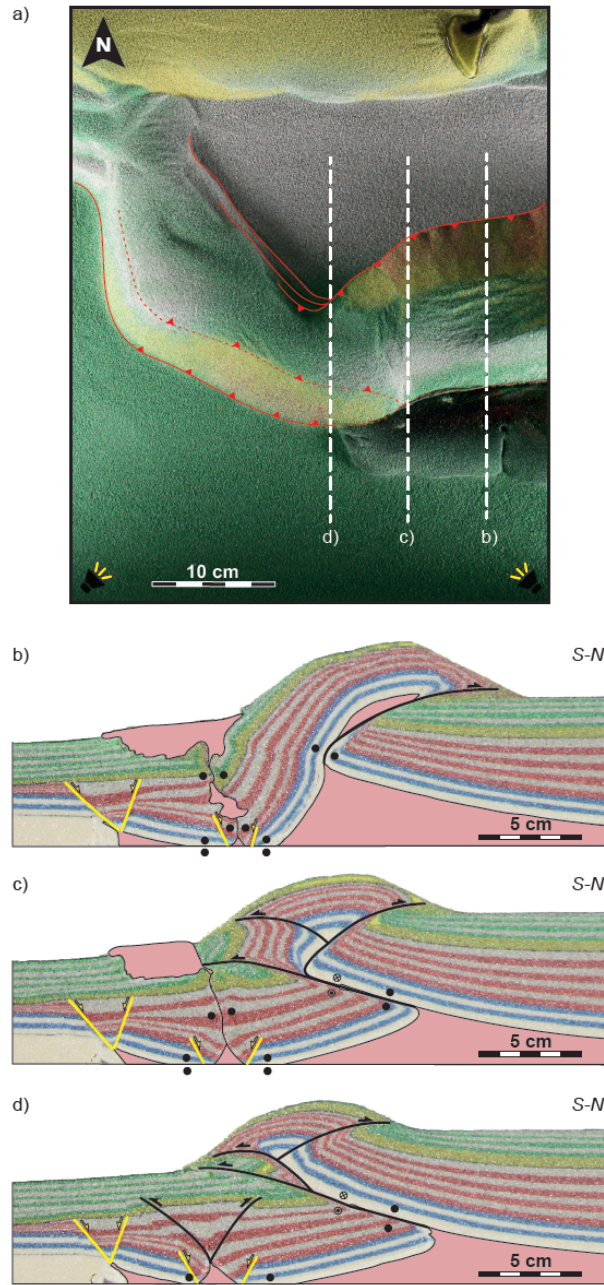
Figure 11: Detailed overhead view of Model-3 at the end of compressional deformation. b) to d) Detailed cross-sections showing the vergence variation between the decoupled and the transitional domains. See section's location in Figure 11a.
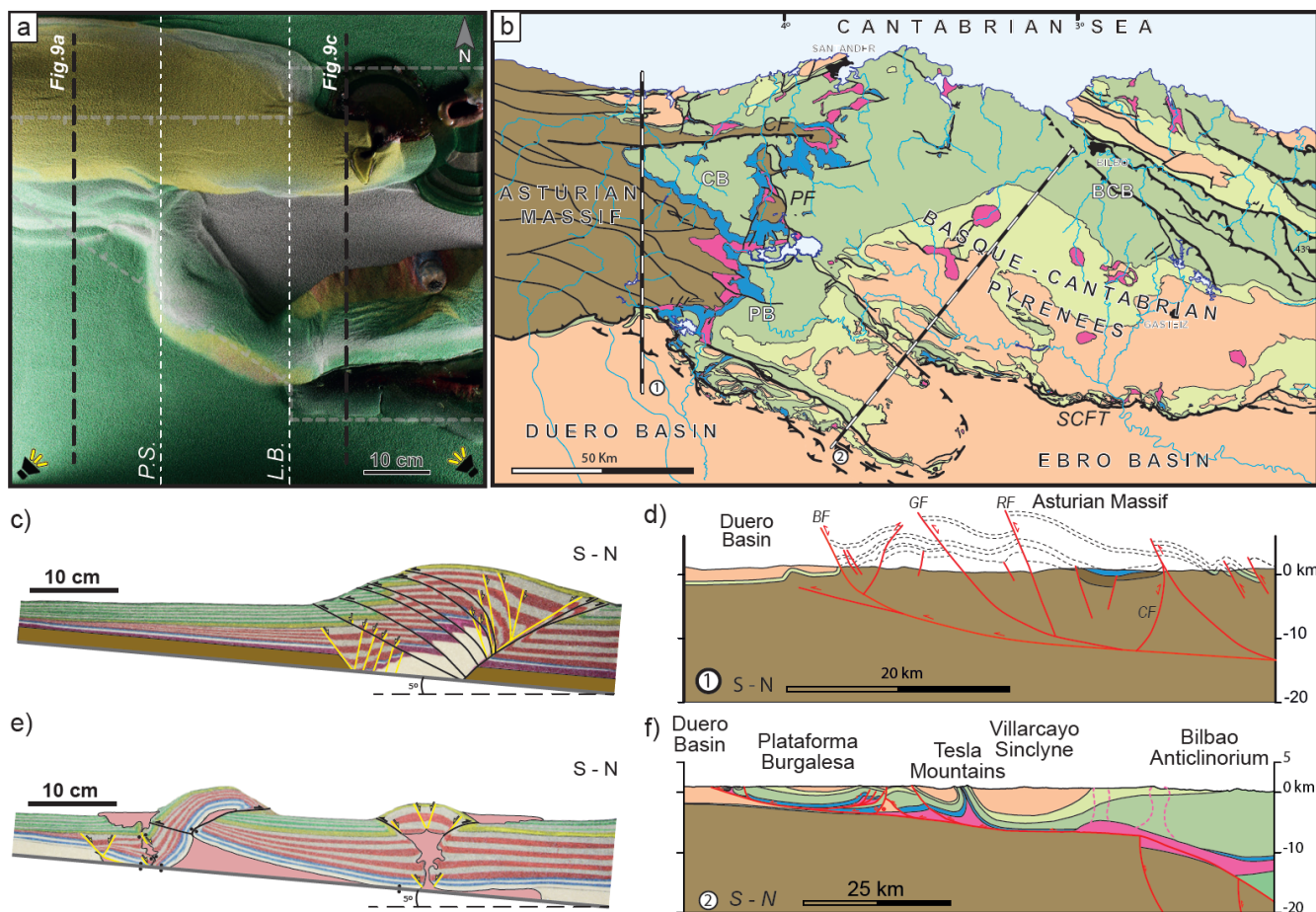
Figure 12: a) Overhead view of Model-3 at the end of the experiment. **b)** Tectonostratigraphic map of the Basque–Cantabrian Pyrenees – Asturian Massif junction (modified from Miró et al., 2021). **c)** Cross-section of the coupled domain showing the thick-skinned deformation in Model-3. **d)** Cross-section through the Asturian Massif (modified from Espina, 1996) showing the thick-skinned deformation similar to what was observed in the model. **e)** Cross-section through the decoupled domain in Model-3. **f)** Cross-section across the southern Basque–Cantabrian Pyrenees showing the characteristic thin-skinned deformation of the area. BF: Becerril Fault, GF: Golobar Fault, RF: Rumaceo Fault, CF: Cabuérniga Fault.